Science Arts & Métiers (SAM)
is an open access repository that collects the work of Arts et Métiers Institute of Technology researchers and makes it freely available over the web where possible.

This is an author-deposited version published in: https://sam.ensam.eu
Handle ID: .http://hdl.handle.net/10985/19198

To cite this version :

Fatima ESSATBI, Justine DELOZANNE, Gurvan MOREAU, Xavier COLIN - Towards a general kinetic model for the thermal oxidation of epoxy-diamine networks. Effect of the molecular mobility around the glass transition temperature - Polymer Degradation and Stability - Vol. 181, p.1-17 - 2020

Any correspondence concerning this service should be sent to the repository Administrator : scienceouverte@ensam.eu

Towards a general kinetic model for the thermal oxidation of epoxy-diamine networks. Effect of the molecular mobility around the glass transition temperature

Xavier Colin[a,*], Fatima Essatbi[a], Justine Delozanne[b], Gurvan Moreau[b]

[a] PIMM, Arts et Métiers Institute of Technology, CNRS, CNAM, HESAM University, 151 boulevard de l'Hôpital, 75013 Paris, France
[b] Safran Composites, A platform of Safran Tech, 33 avenue de la Gare, 91760 Ittevile, France

Keywords:
Epoxy-diamine network
Thermal oxidation
Kinetic model
Oxygen consumption
Carbonyl build-up
Molecular mobility

A B S T R A C T

The kinetic model previously established for describing the thermal oxidation of polymethylenic substrates has been successfully generalized to a series of six epoxy-diamine networks (EPO-DA) characterized by very different glass transition temperatures. This model is derived from the so-called "closed-loop" mechanistic scheme which consists in a radical chain reaction initiated by the decomposition of hydroperoxides and propagating via the C-H bonds located in α of heteroatoms (N and O). The numerous model parameters were determined by applying a "step by step" procedure combining experiment and simulation. On the one hand, oxygen transport properties (i.e. coefficients of oxygen diffusion and solubility) were estimated from a compilation of literature data. On the other hand, rate constants and formation yields were determined by inverse solving method from the measurements of oxygen consumption and carbonyl build-up performed on six different EPO-DA networks between 25 and 200 °C and between 0.16 and 20 bars of oxygen partial pressure in our laboratory or in the literature. It was found that the molecular mobility mainly affects the rate constants of the elementary reactions involving the reactive species in the lowest concentration, i.e. peroxy radicals. In fact, the rate constant k_6 of the apparent termination of peroxy radicals is reduced by about five orders of magnitude when passing from rubbery to glassy state due to the freezing of large amplitude cooperative molecular movements. In contrast, the rate constant k_3 of the propagation of oxidation, involving peroxy radicals but also the polymer substrate, is only changed by one order of magnitude around the glass transition temperature. The introduction of the effect of molecular mobility into the Arrhenius laws of k_6 and k_3 allows building master curves and finally, proposing a single kinetic model for the whole family of EPO-DA networks.

1. Introduction

The vast majority of composite material structures used in the civil aeronautical sector are made of diamine cross-linked epoxy matrix (EPO-DA) reinforced with carbon fibers. The development of a numerical tool for predicting the degradation state of this polymer family under the combined effects of temperature, oxygen and mechanical stress remains an open issue in this sector. Indeed, this tool could help aeronautical manufacturers to take into account the possible alteration of the thermomechanical properties of composite structures from the moment of their design and sizing, but also to consider the use of these materials in more aggressive thermochemical environments.

There is a large amount of literature works devoted to the thermal degradation mechanisms [1-9] and kinetics [10-17] of EPO-DA networks, showing that oxidation is clearly the predominant aging process. However, in these publications, each network is considered as a completely different material from other networks of the EPO-DA family, because it is assumed to be characterized by its own chemistry, its own oxidation mechanisms, its own degradation kinetics and its specific kinetic model. Therefore, the values of the rate constants determined by using these kinetic models as an inverse solving method are found to be quite different, but without giving any real explanation except, perhaps, the possible effect of molecular mobility [15].

However, contrary to popular belief, there are not so great chemical differences between all the networks of the EPO-DA family, especially from a chemical kinetics point of view, as shown in Table 1. Indeed, let us recall that, according to Korcek et al. [18],

* Corresponding author.
E-mail address: xavier.colin@ensam.eu (X. Colin).

Table 1
Main oxidation sites in EPO-DA networks.

Starting epoxy monomer	Oxidation sites
DGEBA, DGEBF, DGEBD, TGPAP, TGTPM, TGMDA, etc…	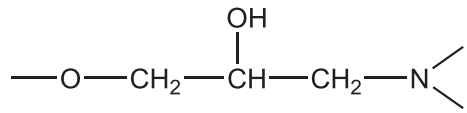
TGPAP and TGMDA only	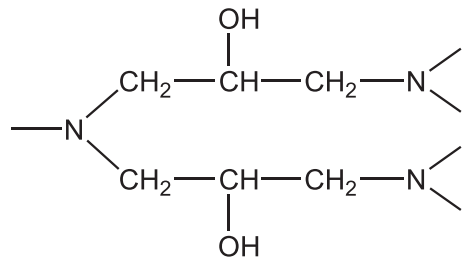

Abbreviations: Diglycidyl ether of bisphenol A (DGEBA), Diglycidyl ether of bisphenol F (DGEBF), Diglycidyl ether of bisphenol D (DGEBD), Triglycidyl ether of para-amino phenol (TGPAP), Triglycidyl ether of triphenyl methane (TGTPM), Tetraglycidyl ether of methylene dianiline (TGMDA).

oxidation propagates via the most labile hydrogens of the constitutive repeating unit. Thus, in EPO-DA networks, the main oxidation sites are oxy-methylene (-O-CH_2-) and amino-methylene (>N-CH_2-) groups, which are already present in the starting epoxy monomers, but also amino-methylene (-CH_2-N<) and methanol groups (>CH-OH) which are formed during the polymerization reaction between the epoxy monomer and diamine hardener. All these oxidation sites are reported in Table 1, as well as the corresponding name of the starting epoxy monomer.

Based on these observations, it is difficult to imagine large fundamental differences between the oxidation mechanisms of the different EPO-DA networks. However, as their glass transition temperature can vary in a wide temperature range, typically between 0 °C and 221 °C [19], it is expected that the molecular mobility plays indeed a key role in their oxidation kinetics, in particular on both sides of the glass transition temperature. In other words, at a same aging temperature, it would not be surprising to find a large difference between the oxidation rates of two EPO-DA networks that are in different physical states (i.e. in glassy and rubbery states). Unfortunately, until now, there are too few experimental data available in the literature on the thermal oxidation of EPO-DA networks to doubtless check this assumption. In addition, almost all studies are focused on thermal aging in glassy state that is, of course, the usual temperature range for industrial applications of these materials.

The impact of molecular mobility on the oxidation kinetics was clearly put in evidence for another thermodynamic transition: the melting, in an electron-beam irradiation cross-linked linear polyethylene (XLPE) [20,21]. A jump of about half a decade was observed for the pre-exponential factor around the melting temperature (130 °C) in the Arrhenius diagram of the oxidation induction time. However, this discontinuity is relatively subtle and thus, can be hidden by the wider scattering of experimental data in PE compilations [22].

The effect of glass transition on the oxidation kinetics is expected to be much more marked because all the diffusion processes are favored by large amplitude cooperative molecular movements in rubbery state, whereas they are almost totally frozen in glassy state. In fact, as for a common polymerization reaction, two kinetic regimes should be distinguished: i) One above T_g, for which the reaction kinetics is governed by the intrinsic reactivity of reactive species and thus, can be satisfyingly described by the classical rules of chemical kinetics; ii) Another below T_g, for which the reaction kinetics is governed by the diffusivity of reactive species. This latter regime was specifically investigated by Waite [23] and Russian researchers [24,25].

That is the reason why some aromatic polymers which contains also few hydrocarbon groups reputed to be very easily oxidizable (e.g. methynic and methylenic groups), such as polyimides of poly(bismaleimide) type [26] or polymerization of monomeric reactant (PMR) type [27], can be considered as thermostable in glassy state. This is also the case for many aromatic epoxies [10,28,29].

The present article aims at laying down the main lines of a general kinetic model for the thermal oxidation of networks of the EPO-DA family and checking its validity. After having recalled its theoretical bases and structure, its different parameters will be determined by applying a “step by step” procedure combining experience and simulation. First of all, oxygen transport properties (i.e. coefficients of oxygen diffusion and solubility) will be estimated from a compilation of literature data. Then, rate constants and formation yields will be determined by inverse solving method from the measurements of oxygen consumption and carbonyl build-up performed on six different EPO-DA networks between 25 and 200 °C and between 0.16 and 20 bars of oxygen partial pressure in our laboratory or in literature.

2. Theory

2.1. Oxidation sites

As mentioned in introduction, the main oxidation sites in EPO-DA networks are oxy-methylene (-O-CH_2-), amino-methylene (>N-CH_2-) and methanol groups (>CH-OH) (see Table 1). Indeed, C–H bonds are characterized by a much lower dissociation energy ($E_D \approx 376$ kJ.mol^{-1}) when they are located in α of a heteroatom (O or N) rather than in polymethylenic sequences ($E_D \approx 393$ kJ.mol^{-1}) [30]. Table 2 recalls the Arrhenius parameters and orders of magnitude at 30 °C of the rate constant k_3 for the propagation of oxidation determined in the previous studies conducted in our laboratory [22,31-37].

Table 2
Arrhenius parameters and orders of magnitude at 30 °C of the rate constant k_3 for the propagation of oxidation on the main types of methylenic C–H bonds.

C-H bond	k_{30} (L.mol^{-1}.s^{-1})	E_3 (kJ.mol^{-1})	k_3 at 30 °C (L.mol^{-1}.s^{-1})	Polymer	References
$-CH_2-CH_2-$	1.5×10^{10}	73	4.0×10^{-3}	PE	[22,31,32]
	9.9×10^{10}	78	3.6×10^{-3}	EPDM	[33]
$-CH{=}CH-CH_2-$	4.0×10^{9}	68	7.7×10^{-3}	BR	[34]
$-O-CH_2-$	1.8×10^{9}	63	2.5×10^{-2}	PET, EPO-AN	[35,36]
$>N-CH_2-$	1.8×10^{9}	63	2.5×10^{-2}	PA 6–6	[37]

Abbreviations: Polyethylene (PE), Ethylene-Propylene terpolymer (EPDM), Polybutadiene (BR), Poly(ethylene terephthalate) (PET), Anhydride cross-linked epoxy (EPO-AN), Polyamide 6–6 (PA 6–6).

Thus, as linear polyesters [35], epoxy-anhydride networks [36] and aliphatic polyamides [37], EPO-DA networks will be subjected to a much more severe oxidation than PE [22,31,32].

2.2. Mechanistic scheme

The so-called "closed-loop" oxidation mechanism, developed for polymethylenic substrates in previous studies [22,31-37], was naturally chosen for EPO-DA networks in the present study. Its generalization to EPO-DA networks required a re-adjustment in the consumption yields of PH substrate in the different balance reactions (i.e. involving several elementary chemical events). Its final version, already detailed and explained in reference [37], is given below:

Initiation:

1u) $POOH \rightarrow 2P^{\bullet} + (1-\gamma_{CO})P\text{-}OH + \gamma_{CO}P{=}O + \gamma_1 S\ \{-(2+\gamma_1)PH\}\ (k_{1u})$

1b) $2POOH \rightarrow P^{\bullet} + PO_2{}^{\bullet} + (1-\gamma_{CO})P\text{-}OH + \gamma_{CO}P{=}O + \gamma_1 S\ \{-(1+\gamma_1)PH\}\ (k_{1b})$

Propagation:

2) $P^{\bullet} + O_2 \rightarrow PO_2{}^{\bullet}\ (k_2)$

3) $PO_2{}^{\bullet} + PH \rightarrow POOH + P^{\bullet}\ (k_3)$

(Terminating and non-terminating) bimolecular combinations:

4) $P^{\bullet} + P^{\bullet} \rightarrow \gamma_4 P\text{-}P + (1-\gamma_4)PH + (1-\gamma_4)F + \gamma_4 B\ \{+(1-\gamma_4)PH\}\ (k_4)$

5) $P^{\bullet} + PO_2{}^{\bullet} \rightarrow \gamma_5 POOP + (1-\gamma_5)POOH + (1-\gamma_5)F + \gamma_5 B\ (k_5)$

6a) $PO_2{}^{\bullet} + PO_2{}^{\bullet} \rightarrow [PO^{\bullet\bullet}OP]_{cage} + O_2\ (k_{6a})$

6b) $[PO{\bullet\bullet}OP]_{cage} \rightarrow POOP + B\ (k_{6b})$

6c) $[PO^{\bullet\bullet}OP]_{cage} \rightarrow P\text{-}OH + P{=}O\ (k_{6c})$

6d) $[PO^{\bullet\bullet}OP]_{cage} \rightarrow 2P^{\bullet} + 2(1-\gamma_{CO})P\text{-}OH + 2\gamma_{CO}P{=}O + 2\gamma_1 S\ \{-2(1+\gamma_1)PH\}\ (k_{6d})$

where PH; POOH; $P^{\bullet}$, $PO_2{}^{\bullet}$ and $PO^{\bullet}$; POOP, P-OH and P=O; F; S and B designate an oxidation site; an hydroperoxide; alkyl, peroxy and alkoxyl radicals; peroxide, hydroxyl and carbonyl groups; a double bond; a chain scission and a crosslink node, respectively. k_i are the reaction rate constants and γ_i are the formation yields of the different inactive products in the corresponding balance reactions.

Very briefly, let us recall the main characteristics of this oxidation mechanism:

i) The propagation of oxidation, by abstracting the most labile hydrogen atoms (3), leads to the formation of a very instable species: hydroperoxide group POOH. Indeed, the dissociation energy of the O–O bond is extremely low: $E_D \approx 150$ kJ.mol^{-1}, against more than 280 kJ.mol^{-1} for all other chemical bonds (i.e. C–O, C–N, C–C and C–H) composing the EPO-DA networks [30]. Therefore, this main propagation product will be, either from the starting of exposure, or very quickly, the main source of radicals. This "closed loop" character allows accounting for the sudden and sharp auto-acceleration of oxidation at the end of an incubation period, commonly called the "induction period" [38]. It is noteworthy that, in the kinetic model, the initial hydroperoxide concentration $[POOH]_0$ is kinetically equivalent to all structural defects (e.g. oxidation products formed during the polymerization reaction of the macromolecular network) and intrinsic species (e.g. catalytic residues, PH-O_2 complexes, other impurities, etc.) responsible for the very first oxidation events.

ii) The thermal decomposition of POOH occurs in two modes: unimolecular (1u) and bimolecular (1b). When the polymer is not too pre-oxidized (i.e. when $[POOH]_0 < [POOH]_C$), the POOH decomposition starts in unimolecular mode. Then, when [POOH] exceeds a critical value $[POOH]_C$, which is a decreasing function of temperature obeying an Arrhenius law, the bimolecular decomposition becomes in turn the predominant mode. For EPO-DA networks, it was found that: $[POOH]_C = 6.8 \times 10^3 \mathrm{Exp}(-40,000/RT)$. On the contrary, when $[POOH]_0 > [POOH]_C$, oxidation is initiated by the bimolecular mode throughout the exposure duration. This is generally the case for all polymers at low temperatures (typically for T < 100 °C).

iii) The writing of the two initiations (1u and 1b) can be surprising due to the apparent non-compliance with stoichiometry. In fact, these initiations are balance reactions involving several elementary chemical events. Their writing will not be detailed here, but the reader can consult reference [37] for further details. Let us just point out that this writing is entirely justified because the dissociation of O–O bond is the limiting step. In addition, the same formation yields can be used for the different inactive products (P-OH, P=O and S) because they result from the same reactive species ($PO^{\bullet}$ and PH) involved in these two initiations. However, due to the ignorance of the exact nature of carbonyl group P=O and thus, the value of its molar extinction coefficient, it was necessary to introduce an apparent formation yield γ_{CO} and to distinguish it from the actual yield of chain scissions γ_1. The same considerations apply to the non-terminating bimolecular combination (6d).

iv) Terminations between two alkyl radicals $P^{\bullet}$ (4) or between one alkyl $P^{\bullet}$ and one peroxy radical $PO_2{}^{\bullet}$ (5) are also balance reactions. Indeed, these two reactions involve two elementary chemical events: coupling and disproportionation. Thus, γ_4 and γ_5 are the formation yields in crosslink nodes.

v) In fact, the combination between two peroxy radicals $PO_2{}^{\bullet}$ (6) involves four competitive elementary chemical events (6a to 6d). This writing allowed highlighting the existence of a non-terminating combination, but also better distinguishing crosslinking B from chain scissions S. Indeed, in polymethylenic substrates, the termination of $PO_2{}^{\bullet}$ is not very efficient [39,40]. As an example, it was found that about 70 and 85% of alkoxyl radicals escape from the cage to initiate new radical oxidation chains at 160 °C in PE and PA 6–6, respectively [37]. However, for a sake of simplicity, these four chemical events can be grouped into a single appar-

ent terminating combination ($PO_2^{\bullet} + PO_2^{\bullet} \rightarrow$ inactive products $+ O_2$) whose the corresponding rate constant k_6 can be expressed as a function of all elementary rate constants, as follows [22]:

$$k_6 = \frac{2(k_{6b} + k_{6c})^2 k_{6a}}{(k_{6b} + k_{6c} + k_{6d})(2k_{6b} + k_{6c} + k_{6d})} \quad (1)$$

vi) Finally, it is noteworthy that inactive molecular (P-OH and P=O) and macromolecular products (S and B) are exclusively formed in initiations (1u and 1b) and in the (terminating and non-terminating) bimolecular combinations of peroxy radicals (6c and 6d).

2.3. 2.3 Kinetic model

A system of ten non-linear differential equations (SED) was derived from the previous mechanistic scheme using the classical rules of the chemical kinetics. This system gives access to the local concentration changes of all the reactive species involved in the mechanistic scheme (i.e. [POOH], $[P^{\bullet}]$, $[PO_2^{\bullet}]$, $[PO^{\bullet\bullet}OP]_{cage}$, [PH] and $[O_2] = f(z, t)$), but also to the local concentration changes of the most important inactive products from a practical point of view, as they can be easily measured experimentally. In this study, we focused on oxygen consumption ($[O_{2\ abs}]$), carbonyl groups ([P=O]) and macromolecular modifications (i.e. B and S). In the case of one-dimensional oxygen diffusion (e.g. through the sample thickness), the resulting SED can be written as follows:

$$\frac{d[POOH]}{dt} = -k_{1u}[POOH] - 2k_{1b}[POOH]^2 + k_3[PO_2^{\bullet}][PH] + (1-\gamma_5)k_5[P^{\bullet}][PO_2^{\bullet}] \quad (2)$$

$$\frac{d[P^{\bullet}]}{dt} = 2k_{1u}[POOH] + k_{1b}[POOH]^2 - k_2[P^{\bullet}][O_2] + k_3[PO_2^{\bullet}][PH] - 2k_4[P^{\bullet}]^2 - k_5[P^{\bullet}][PO_2^{\bullet}] + 2k_{6d}[PO^{\bullet}OP]_{cage} \quad (3)$$

$$\frac{d[PO_2^{\bullet}]}{dt} = k_{1b}[POOH]^2 + k_2[P^{\bullet}][O_2] - k_3[PO_2^{\bullet}][PH] - k_5[P^{\bullet}][PO_2^{\bullet}] - 2k_{6a}[PO_2^{\bullet}]^2 \quad (4)$$

$$\frac{d[PO^{\bullet\bullet}OP]_{cage}}{dt} = k_{6a}[PO_2^{\bullet}]^2 - (k_{6b} + k_{6c} + k_{6d})[PO^{\bullet\bullet}OP]_{cage} \quad (5)$$

$$\frac{d[PH]}{dt} = -(2+\gamma_1)k_{1u}[POOH] - (1+\gamma_1)k_{1b}[POOH]^2 - k_3[PO_2^{\bullet}][PH] - 2(1+\gamma_1)k_{6d}[PO^{\bullet\bullet}OP]_{cage} \quad (6)$$

$$\frac{d[O_2]}{dt} = D_{O2}\frac{\partial^2[O_2]}{\partial z^2} - k_2[P^{\bullet}][O_2] + k_{6a}[PO_2^{\bullet}]^2 \quad (7)$$

$$\frac{d[O_{2\ abs}]}{dt} = R_{O2} = k_2[P^{\bullet}][O_2] - k_{6a}[PO_2^{\bullet}]^2 \quad (8)$$

$$\frac{d[P=O]}{dt} = \gamma_{CO}k_{1u}[POOH] + \gamma_{CO}k_{1b}[POOH]^2 + (k_{6c} + 2\gamma_{CO}k_{6d})[PO^{\bullet\bullet}OP]_{cage} \quad (9)$$

$$\frac{dS}{dt} = \gamma_1 k_{1u}[POOH] + \gamma_1 k_{1b}[POOH]^2 + 2\gamma_1 k_{6d}[PO^{\bullet\bullet}OP]_{cage} \quad (10)$$

$$\frac{dB}{dt} = \gamma_4 k_4[P^{\bullet}]^2 + \gamma_5 k_5[P^{\bullet}][PO_2^{\bullet}] + k_{6b}[PO^{\bullet\bullet}OP]_{cage} \quad (11)$$

where D_{O2} is the coefficient of oxygen diffusion into the EPO-DA network and z is the spatial co-ordinate (i.e. the depth beneath the sample surface). R_{O2} is the rate of oxygen chemical consumption, commonly called the "oxidation rate".

This SED was solved simultaneously in space (z) and time (t) with numerical algorithms specifically recommended for "stiff problems" of chemical kinetics [41], as already reported in many previous papers, for instance in reference [42].

Initial and boundary conditions were:

i) When t = 0, at any depth z in the sample thickness:

$[POOH](z,\ 0) = [POOH]_0 = 10^{-4}\ mol.L^{-1}$

$[P^{\bullet}](z,\ 0) = [PO_2^{\bullet}](z,\ 0) = [PO^{\bullet\bullet}OP]_{cage}(z,\ 0) = 0$

$[PH](z,\ 0) = [PH]_0$

and $[O_2](z,\ 0) = [O_2]_0$

ii) When $t \geq 0$, on both sample surfaces ($z = \pm L$):

$[O_2](-L,\ t) = [O_2](+L,\ 0) = [O_2]_0$

Oxygen concentration obeys the classical Henri's law:

$$[O_2]_0 = S_{O2}\ .\ P_{O2} \quad (12)$$

where S_{O2} is the coefficient of oxygen solubility into the EPO-DA network and P_{O2} is the oxygen partial pressure in the exposure environment. The sample thickness is 2L.

3. Materials and experimental procedure

3.1. EPO-DA networks

The study focused on six perfect EPO-DA networks (i.e. without dangling chains) characterized by very different glass transition temperatures, typically ranged between 95 and 263 °C (see Table 3).

Four of them result from the reaction of common bi-functional or tri-functional epoxy monomers with an aromatic diamine hardener: 9,9-bis(3-chloro-4-aminophenyl)fluorene (CAF) or 4,4′-diamino diphenyl sulfone (DDS). Over the past twenty years, these four networks were all considered, in turn, as potential matrices of carbon fiber reinforced composite materials for structural applications at low to moderate temperatures (typically between 70 °C and 150 °C) in the civil aeronautical sector. The marketing of network no. 5 was progressively abandoned in the early 2000s, but its thermal degradation between 150 °C and 210 °C was the subject of several papers a few years earlier, for instance [10-14]. Network no. 6 was considered in the early 2010s for applications at temperatures above 200 °C, for which there is clearly a lack of solutions in organic materials in Europe. Its thermal degradation was also the subject of few papers, for instance [15,16]. In contrast, networks no. 3 and 4 are completely new materials whose the thermal aging behaviors have not still been published to date.

Films of these four EPO-DA networks, with thicknesses typically ranging between 25 and 100 µm, were produced by compression molding then post-cured under primary vacuum (i.e. 10^{-3} bar) in accordance with the recommended industrial cure cycle, in order to reach the maximum crosslinking density while avoiding any undesired pre-oxidation before exposure to thermal aging. That is the reason why a very low concentration in structural defects will be chosen for modeling the thermal aging kinetics of these networks in the present study, typically: $[POOH]_0 = 10^{-4}\ mol.l^{-1}$.

After processing, the films were characterized by conventional laboratory techniques. In particular, their glass transition temperature (T_g) was determined by differential scanning calorimetry (DSC, with a 20 °C.min^{-1} heating rate, under nitrogen) and confirmed by mechanical spectrometry (DMA, in tensile mode, with a 1 Hz frequency and a 2 °C.min^{-1} heating rate, under nitrogen). The measurements were found very close to the theoretical values of T_g determined with the Di Marzio's equation [43] for perfect networks

Table 3
Molar mass of the repetitive monomer unit (m_{UCR}), density (ρ) and concentration in oxidation sites (PH) for perfect EPO-DA networks.

Number	Network	m_{UCR} (g.mol^{-1})	ρ	[PH] (mol.L^{-1})	T_g (°C)
1	Epon 828-Jeffamine D230	910	1.16	24.2	95
2	Epon 828-Ancamine 2049	918	1.2	32.7	150–155
3	DGEBF-CAF	1041	1.25	14.4	158
4	DGEBA-CAF	1097	1.25	13.7	182
5	[(a)] DGEBF/TGPAP-DDS	1362	1.31	15.4	211
6	[(b)] Tactix 123/Tactix 742-DDS	1674	1.11	10.6	263

Abbreviations: Diglycidyl ether of bisphenol A (DGEBA, Epon 828 or Tactix 123), Diglycidyl ether of bisphenol F (DGEBF), Triglycidyl ether of para-amino phenol (TGPAP), Triglycidyl ether of triphenyl methane (TGTPM or Tactix 742), poly(oxypropylene)diamine (Jeffamine D230), diamino dimethyl dicyclohexyl methane (Ancamine 2049), 9,9-bis(3-chloro-4-aminophenyl)fluorene (CAF), 4,4′-Diamino diphenyl sulfone (DDS).
[(a)] Matrix commercialized under the reference 977–2 by Cytec Fiberite.
[(b)] Matrix commercialized under the name Tactix by Hunstman.

(i.e. without dangling chains). As an example, the method for the T_g calculation of network no. 6 is detailed in reference [29].

In addition, EPO-DA networks no. 1 and 2, resulting from the reaction of diglycidyl ether of bisphenol A (Epon 828) with an aliphatic diamine hardener: poly(oxypropylene) diamine (Jeffamine D230) and diamino dimethyl dicyclohexyl methane (Ancamine 2049) respectively, were considered in the present study for two main reasons:

i) Their T_g is lower than those of all previous networks (see Table 3), thus allowing to analyze the possible effect of molecular mobility on the oxidation kinetics over a wider temperature range;
ii) Their oxygen consumption kinetics was meticulously measured in real time at moderate to very low temperatures close to ambient (typically between 140 °C and 25 °C) [44].

The concentration in oxidation sites [PH] was estimated from the knowledge of the repetitive monomer unit of the six perfect EPO-DA networks. In Table 3, it can be seen that [PH] is significantly higher for epoxies cross-linked with an aliphatic (typically, between 24 and 33 mol.L^{-1}) than an aromatic diamine (between 10 and 15 mol.L^{-1}), which might already explain a significant difference in oxidizability between these two subfamilies of EPO-DA networks. It should be pointed out that, when DDS is the crosslinking agent, the sulfonyl group protects the amino-methylene groups (-CH_2-N<), formed during the polymerization reaction, against the radical attack from oxidation. Indeed, the sulfonyl group is a high electron-attracting group whose the inductive effect through the aromatic rings of DDS leads to an increase in the strength of the C–H bond. This stabilizing effect of sulfonyl group was first evidenced by comparing the polymerization kinetics of different epoxy-diamine mixtures [45]. This is the reason why [PH] is only about 10 mol.L^{-1} for network no. 6.

3.2. Thermal aging and experimental procedures

The oxidation kinetics of networks no. 3, 4 and 6 was studied at 120, 150, 180 and 200 °C under an oxygen partial pressure ranged between 0.21 (ambient air) and 20 bars in autoclaves. Given the high impact of oxygen partial pressure on the oxidation kinetics, the aging experiments at the highest temperature (200 °C) were limited to a maximum pressure of 1 bar so as not to observe high conversion ratios of oxidation from the very first samplings. At the opposite, at the lowest temperatures (120 and 150 °C), the aging experiments were carried out above 0.21 bar in order to detect significant structural modifications after a minimum duration of 3 months. All the films were periodically removed from the aging chambers and cooled to room temperature

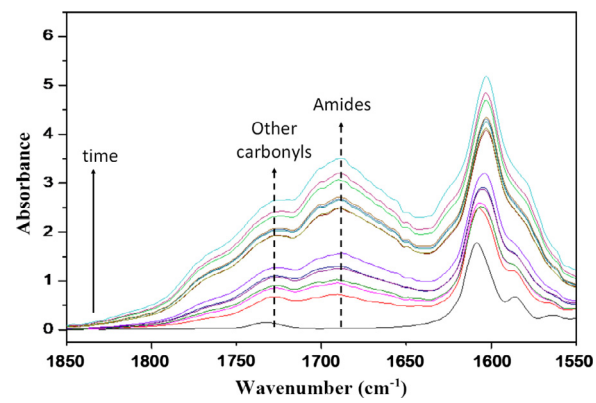

Fig. 1. Changes in the FTIR spectrum of network no. 3 during its thermal aging at 150 °C under 0.21 bar of oxygen (i.e. ambient air). The final spectrum (in sky blue) was recorded after 156 hours of thermal exposure.

in a desiccator containing silica gel for preventing any moisture recovery prior to be characterized by FTIR spectrophotometry. The FTIR spectra were recorded in a transmission mode between 400 and 4000 cm^{-1} with a Perkin Elmer Frontier apparatus, after having averaged the 16 scans obtained with a minimum resolution of 4 cm^{-1}. As reported many times in literature [1-10,46-48], the main structural modifications were observed in the carbonyl region where two new wide absorption bands appeared and grew rapidly with exposure time: one centered around 1680–1690 cm^{-1}, and the other around 1720–1730 cm^{-1}. As an example, Fig. 1 shows the changes over time in the FTIR spectrum of network no. 3 at 150 °C under 0.21 bar of oxygen (i.e. ambient air). These two bands were assigned to amides and other types of carbonyl products, respectively. Unfortunately, the great variety of these latter products (aldehydes, carboxylic acids, phenyl formates, etc.), often resulting from oxidation induced chain scissions in the hydroxyl propyl ether segment [47], did not allow identifying them precisely. Their average concentration throughout the film thickness [P=O] was determined by applying the classical Beer-Lambert's law:

$$[P=O] = \frac{OD}{ep\ \varepsilon} \tag{13}$$

where OD is the optical density of the IR absorption band centered at 1720–1730 cm^{-1} (dimensionless), ε is the corresponding molar extinction coefficient (expressed in L.mol^{-1}.cm^{-1}), and ep is the film thickness (in cm).

For carbonyl products, typical values of ε are ranged between 150 L.mol^{-1}.cm^{-1} (for ketones) and 850 L.mol^{-1}.cm^{-1} (for carboxylic acids) [49-53]. In a first approximation, an average value of 500 L.mol^{-1}.cm^{-1} was chosen for ε in the present study.

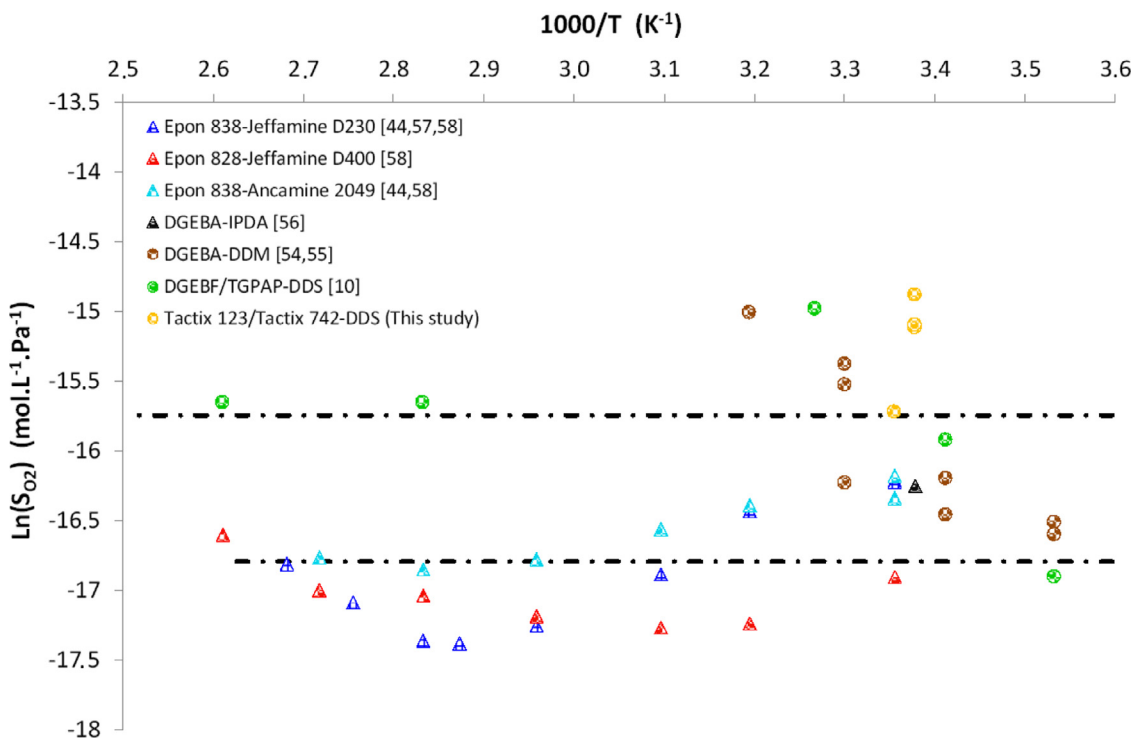

Fig. 2. Arrhenius graph between 10 and 110 °C for the coefficient of oxygen solubility of EPO-DA networks.

The oxidation kinetics of network no. 5 was measured in real time at 180 and 200 °C under an oxygen partial pressure ranged between 0.05 and 1 bar with a homemade thermogravimeter. All details on the apparatus and experimental procedure are available in reference [10].

The oxidation kinetics of networks no. 1 and 2 was measured in real time between 25 and 140 °C under 0.166 bar of oxygen with an ultrasensitive manometric method. All details on the apparatus and experimental procedure are available in reference [44].

4. Kinetic modeling

The first step in kinetic study consisted in the separate determination of the numerous parameters of the kinetic model. These are the seven rate constants (k_{1u}, k_{1b}, k_2, k_3, k_4, k_5 and k_6), the four yields of inactive products formation (γ_1, γ_{CO}, γ_4 and γ_5) and the two oxygen transport properties (S_{O2} and D_{O2}).

4.1. Oxygen transport properties

Figs. 2 and 3 respectively show the compilations of the literature values of S_{O2} and D_{O2} determined by oxygen permeability between 10 and 100 °C for EPO-DA networks [10,44,54-59]. The values measured with Systech 8001 and Mocon Ox-Tran 2–21 devices at room temperature for network no. 6 in our laboratory were added to this compilation.

It clearly appears that S_{O2} erratically varies with temperature. Given the relatively large scattering of the experimental data, it was considered, in first approach, that S_{O2} is independent of temperature. In contrast, D_{O2} significantly increases with temperature and seems to obey an Arrhenius' law. It should be pointed out that, for both oxygen transport properties, no discontinuity is observed when approaching the glass transition temperature.

Two sub-families of EPO-DA networks are clearly put in evidence:

a) For epoxies cross-linked with an aliphatic diamine hardener (Jeffamine D230, Jeffamine D400, Ancamine 2049 or IPDA):

$$S_{O2} \approx 5.1\ 10^{-8}\ \text{mol.L}^{-1}.\text{Pa}^{-1} \tag{14}$$

$$D_{O2} = 3.0\ 10^{-5}\ \text{Exp} - \frac{44\ 600}{RT}\ \text{m}^2.\text{s}^{-1} \tag{15}$$

b) And for epoxies cross-linked with an aromatic diamine hardener (DDM or DDS, but also CAF by generalization):

$$S_{O2} \approx 1.45\ 10^{-7}\ \text{mol.L}^{-1}.\text{Pa}^{-1} \tag{16}$$

$$D_{O2} = 4.7\ 10^{-5}\ \text{Exp} - \frac{20\ 000}{RT}\ \text{m}^2.\text{s}^{-1} \tag{17}$$

Of course, network no. 6 follows this latter behavior. Therefore, it would seem that the presence of aromatic structures, i.e. very rigid structures, in the macromolecular network promotes the dissolution of oxygen, but also considerably slows down its diffusion. At this stage of the investigations, more in-depth studies on a series of model networks are necessary to elucidate the relationships between the molecular and macromolecular structures of EPO-DA networks and their oxygen transport properties.

4.2. Rate constants and formation yields

Rate constants and formation yields were determined by inverse solving method, in particular by simulating as closely as possible the measurements of carbonyl build-up and oxygen consumption of the six EPO-DA networks under study. Given the very large number of parameters to be determined, it was decided to apply a "step by step" procedure.

In a first step, as the main oxidation sites are C-H bonds located in α of heteroatoms (N and O), the values determined for aliphatic polyamides in a previous study [37] were attributed to the rate constants of EPO-DA networks. However, it should be recalled that all these values were determined in rubbery state, while the EPO-DA networks under study are mainly in glassy state. Therefore, in

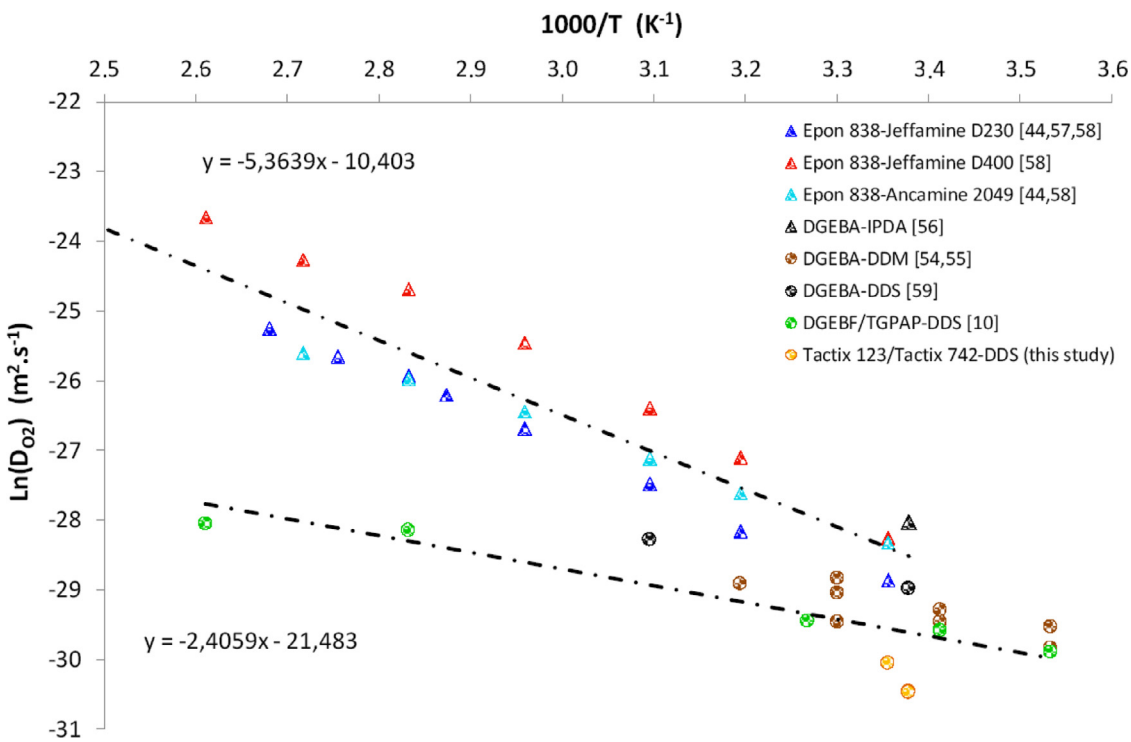

Fig. 3. Arrhenius graph between 10 and 110 °C for the coefficient of oxygen diffusion of EPO-DA networks.

a second step, it was necessary to gradually modify some rate constants, in particular those for which the corresponding reactions involve reactive species in very low concentration, such as peroxy radicals $PO_2^{\bullet}$. Indeed, it was expected that these rate constants would be directly impacted by the freezing of large amplitude cooperative molecular movements, which characterize the main mechanical relaxation α associated to glass transition. In order of priority, these are the rate constants k_{6i} of the (terminating and non-terminating) bimolecular combinations, then the rate constant k_3 of the propagation of oxidation, because this latter only involves one $PO_2^{\bullet}$ radical.

Figs. 4 and 5 show two examples of numerical simulations in glassy state at temperatures well below the glass transition temperature (typically when $T < T_g - 60$ °C). Carbonyl build-up was calculated with Eq. (9) at 150 °C between 0.21 and 20 bars of oxygen (Fig. 4), and between 120 and 200 °C under 0.21 bar of oxygen for network no. 6 (Fig. 5). It can be seen that the kinetic model satisfyingly accounts for both the effects of oxygen partial pressure and temperature on the oxidation kinetics of this EPO-DA network.

The rate constants and formation yields used for these simulations are reported in Table 4. In addition, the values found at 150 °C for aliphatic polyamides in a previous study [37] are given for information. Indeed, these latter will be very helpful for the following discussion, because they were obtained in rubbery state, well above the glass transition temperature of these materials (typically when $T \geq T_g + 100$ °C).

All these values call for several comments:

i) For network no. 6, the initiation rate constants (k_{1u} and k_{1b}) are about 3–4 times higher compared to aliphatic polyamides throughout the temperature range under investigation. This result suggests a higher instability of hydroperoxides in EPO-DA networks presumably due to the presence of heteroatoms (N or O) in a β position (see Table 1). As it will be seen in the next Tables 5 and 6, this is general behavior for EPO-DA networks. The Arrhenius laws found for k_{1u} and k_{1b} for the whole family of EPO-DA networks throughout the 25–200 °C interval are:

$$k_{1u} = 1.3\ 10^{13}\ \mathrm{Exp} - \frac{130\ 000}{RT} s^{-1} \quad (16)$$

and

$$k_{1b} = 1.9\ 10^{9}\ \mathrm{Exp} - \frac{90\ 000}{RT} L.mol^{-1}.s^{-1} \quad (17)$$

ii) For network no. 6, the rate constant k_6 of apparent termination of peroxy radicals is five orders of magnitude lower compared to aliphatic polyamides throughout the temperature range under investigation. This large gap was mainly attributed to the effect of molecular mobility on the bimolecular combinations of peroxy radicals on both sides of the glass transition temperature. In contrast and as expected, the impact of molecular mobility on the propagation of oxidation is much more moderate. Indeed, for network no. 6, the rate constant k_3 is only two orders of magnitude lower compared to aliphatic polyamides.

iii) The formation yield in carbonyls γ_{CO} is quite different between network no. 6 and aliphatic polyamides throughout the temperature range under investigation. This difference could be explained by the formation of a much greater variety of carbonyl products in EPO-DA networks. In addition, as the relative predominance between these different carbonyl products depends on temperature, γ_{CO} varies throughout the temperature interval under investigation. The fact that γ_{CO} decreases with temperature just confirms that aldehydes are much less oxidizable at low temperature. As a consequence, the average molar extinction coefficient ε, used to estimate the global concentration of carbonyl products from FTIR measurements (see Eq. 13), should be progressively decreased with temperature in order to take into account this changes in the chemical composition. As it will be seen in the next Table 5, this also seems to be a general behavior for EPO-DA networks.

iv) All other rate constants (k_2, k_4 and k_5) and formation yields (γ_1, γ_4 and γ_5) were kept identical, if not very close, to

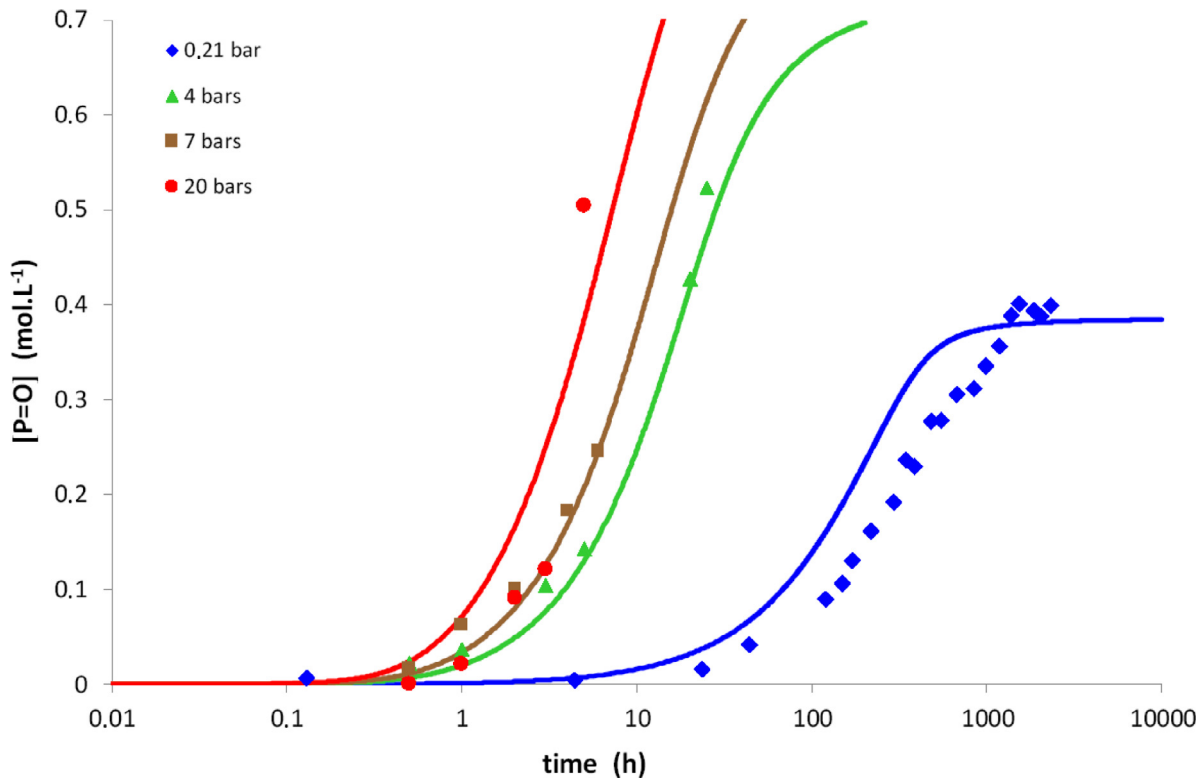

Fig. 4. Carbonyl build-up in 100 µm thick films of network no. 6 (Tactix 123/Tactix 742-DDS) at 150 °C between 0.21 and 20 bars of oxygen. Comparison between simulations with Eq. (9) (solid lines) and experimental data (points).

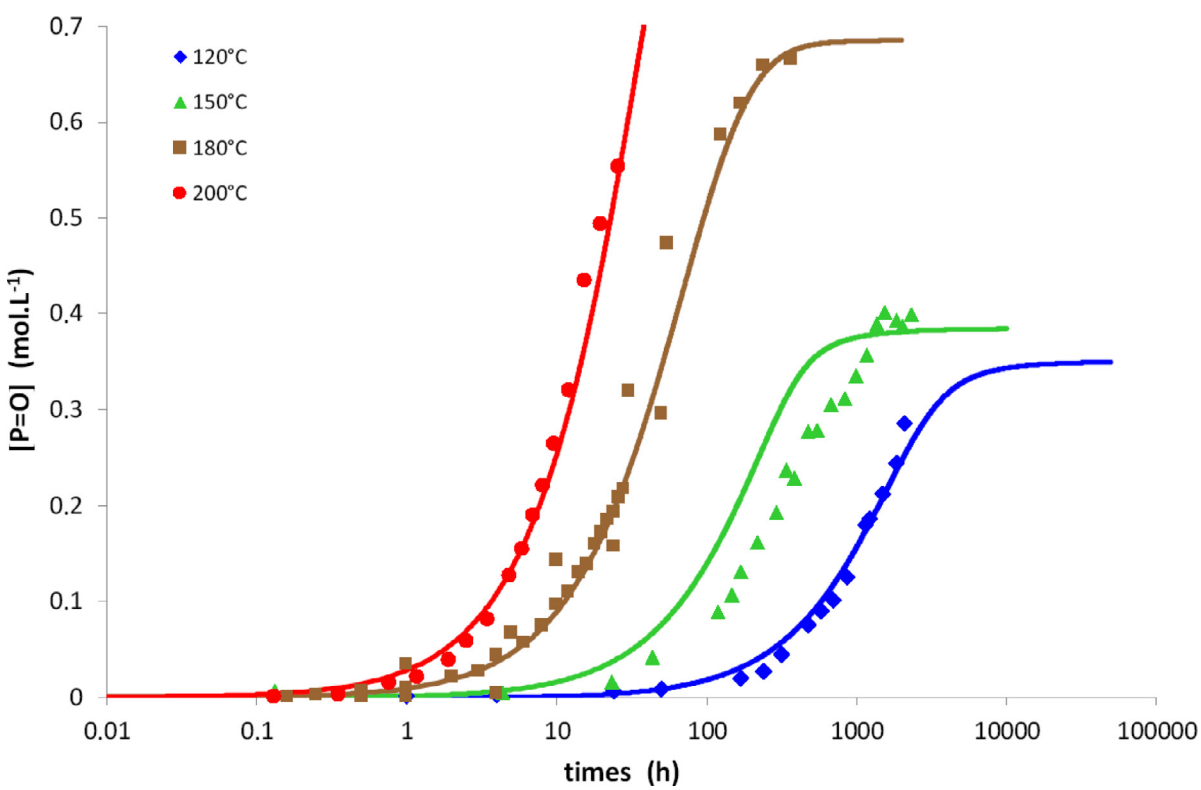

Fig. 5. Carbonyl build-up in 100 µm thick films of network no. 6 (Tactix 123/Tactix 742-DDS) between 120 and 200 °C under 0.21 bar of oxygen (ambient air). Comparison between simulations with Eq. (9) (solid lines) and experimental data (points).

Table 4
Values of the rate constants and formation yields used for modeling the thermal oxidation kinetics of network no. 6 between 120 and 200 °C. Comparison with the values previously determined at 150 °C for aliphatic polyamides [37].

Polymer	Tactix 123/Tactix 742-DDS [$T_g = 263$ °C]				PA [$T_g \approx 40$–55 °C]
T (°C)	120	150	180	200	150
k_{1u} (s^{-1})	8.0×10^{-5}	1.3×10^{-3}	1.5×10^{-2}	6.5×10^{-2}	4.4×10^{-4}
k_{1b} ($L.mol^{-1}.s^{-1}$)	2.1×10^{-3}	1.5×10^{-2}	8.1×10^{-2}	2.2×10^{-1}	3.5×10^{-3}
k_2 ($L.mol^{-1}.s^{-1}$)	10^8	10^8	10^8	10^8	10^8
k_3 ($L.mol^{-1}.s^{-1}$)	7.0×10^{-2}	2.9×10^{-1}	9.9×10^{-1}	2.0	3.0×10^1
k_4 ($L.mol^{-1}.s^{-1}$)	8.0×10^{11}	8.0×10^{11}	8.0×10^{11}	8.0×10^{11}	8.0×10^{11}
k_5 ($L.mol^{-1}.s^{-1}$)	3.0×10^{11}	3.0×10^{11}	3.0×10^{11}	3.0×10^{11}	5.0×10^{11}
k_6 ($L.mol^{-1}.s^{-1}$)	3.0×10^4	6.8×10^4	8.2×10^4	8.7×10^4	7.4×10^9
γ_1 (%)	60	60	60	60	100
γ_{CO} (%)	8.5	11.2	21.5	33.5	100
γ_4 (%)	50	50	50	50	55
γ_5 (%)	50	50	50	50	55

Table 5
Values of the rate constants and formation yields used for modeling the thermal oxidation kinetics of networks no. 3 and 4 at 120 and 150 °C. Comparison with the values previously determined at 150 °C for aliphatic polyamides [37].

Polymer	DGEBF-CAF [$T_g = 158$ °C]		DGEBA-CAF [$T_g = 182$ °C]		PA [$T_g \approx 40$–55 °C]
T (°C)	120	150	120	150	150
k_{1u} (s^{-1})	8.0×10^{-5}	1.3×10^{-3}	8.0×10^{-5}	1.3×10^{-3}	4.4×10^{-4}
k_{1b} ($L.mol^{-1}.s^{-1}$)	2.1×10^{-3}	1.5×10^{-2}	2.1×10^{-3}	1.5×10^{-2}	3.5×10^{-3}
k_2 ($L.mol^{-1}.s^{-1}$)	10^8	10^8	10^8	10^8	10^8
k_3 ($L.mol^{-1}.s^{-1}$)	2.5×10^{-1}	3.0	3.1×10^{-1}	2.0	3.0×10^1
k_4 ($L.mol^{-1}.s^{-1}$)	8.0×10^{11}	8.0×10^{11}	8.0×10^{11}	8.0×10^{11}	8.0×10^{11}
k_5 ($L.mol^{-1}.s^{-1}$)	3.0×10^{11}	3.0×10^{11}	3.0×10^{11}	3.0×10^{11}	5.0×10^{11}
k_6 ($L.mol^{-1}.s^{-1}$)	7.7×10^4	4.3×10^6	5.5×10^4	3.0×10^5	7.4×10^9
γ_1 (%)	60	60	60	60	100
γ_{CO} (%)	25	30	30	35	100
γ_4 (%)	50	50	50	50	55
γ_5 (%)	50	50	50	50	55

Table 6
Values of the rate constants and formation yields used for modeling the thermal oxidation kinetics of networks no. 1 and 2 at 125 and 140 °C, and network no. 5 at 180 and 200 °C.

Network	Epon 828-Jeffamine D230 [$T_g = 95$ °C]		Epon 828-Ancamine 2049 [$T_g = 150$–155 °C]		DGEBF/TGPAP-DDS [$T_g = 211$ °C]	
T (°C)	125	140	125	140	180	200
k_{1u} (s^{-1})	1.3×10^{-4}	5.4×10^{-4}	1.3×10^{-4}	5.4×10^{-4}	1.5×10^{-2}	6.4×10^{-2}
k_{1b} ($L.mol^{-1}.s^{-1}$)	3.0×10^{-3}	8.0×10^{-3}	3.3×10^{-3}	8.0×10^{-3}	8.1×10^{-2}	2.2×10^{-1}
k_2 ($L.mol^{-1}.s^{-1}$)	10^8	10^8	10^8	10^8	10^8	10^8
k_3 ($L.mol^{-1}.s^{-1}$)	2.1	4.6	3.0×10^{-1}	7.0×10^{-1}	8.0×10^{-1}	3.0
k_4 ($L.mol^{-1}.s^{-1}$)	8.0×10^{11}	8.0×10^{11}	8.0×10^{11}	8.0×10^{11}	8.0×10^{11}	8.0×10^{11}
k_5 ($L.mol^{-1}.s^{-1}$)	3.0×10^{11}	3.0×10^{11}	3.0×10^{11}	3.0×10^{11}	3.0×10^{11}	3.0×10^{11}
k_6 ($L.mol^{-1}.s^{-1}$)	2.9×10^9	6.9×10^9	6.5×10^5	9.9×10^6	1.7×10^6	2.7×10^7
γ_1 (%)	60	60	60	60	100	100
γ_4 (%)	50	50	50	50	55	55
γ_5 (%)	50	50	50	50	55	55

the values of aliphatic polyamides [37]. As it can be noted in Tables 4, 5 and 6, all these parameters are independent of temperature.

Figs. 6 and 7 show two examples of numerical simulations still in glassy state, but now, up to temperatures near the glass transition temperature (typically for T_g – 60 °C < T ≤ T_g – 10 °C). Carbonyl build-ups were calculated with Eq. (9) at 120 and 150 °C between 0.21 and 10 bars of oxygen for networks no. 3 and 4. Here also, it can be seen that the kinetic model satisfyingly accounts for both the effects of the oxygen partial pressure and temperature on the oxidation kinetics of these two EPO-DA networks, despite a slightly larger scattering of experimental results.

The rate constants and formation yields used for all these simulations are reported in Table 5. In addition, the values found at 150 °C for aliphatic polyamides in a previous study [37] are recalled for information.

These new results call for the following additional comments. As expected, the impact of the molecular mobility on the bimolecular combinations of peroxy radicals and the propagation of oxidation is significantly reduced when increasing the exposure temperature and approaching the glass transition temperature of both EPO-DA networks. As an example, at T = T_g – 30 °C for network no. 3, k_6 is only three orders of magnitude lower compared to aliphatic polyamides (against five orders of magnitude when T < T_g – 60 °C). Similarly, at T = T_g – 30 °C for network no. 3, k_3 is only one order of magnitude lower compared to aliphatic polyamides (against three when T < T_g – 60 °C).

Finally, Fig. 8 shows one example of numerical simulations on both sides of the glass transition temperature (typically when T_g –

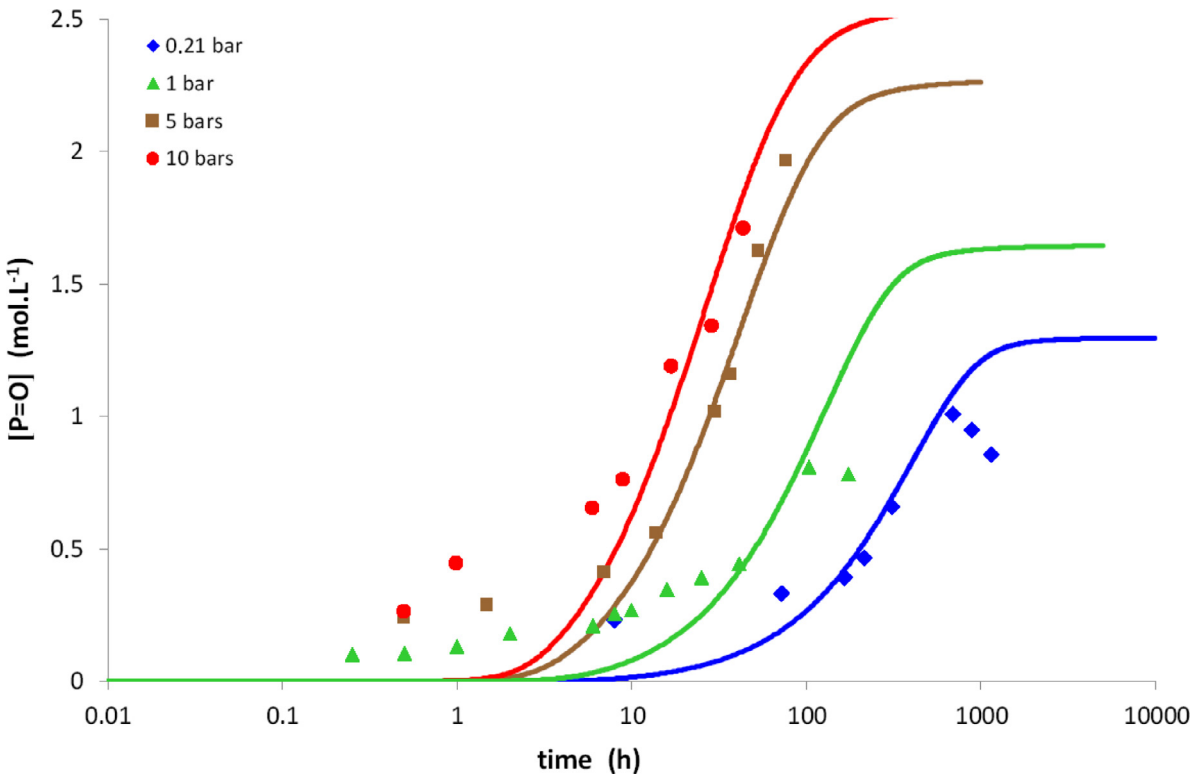

Fig. 6. Carbonyl build-up in 25 µm thick films of network no. 4 (DGEBA-CAF) at 120 °C between 0.21 (ambient air) and 10 bars of oxygen. Comparison between simulations with Eq. (9) (solid lines) and experimental data (points).

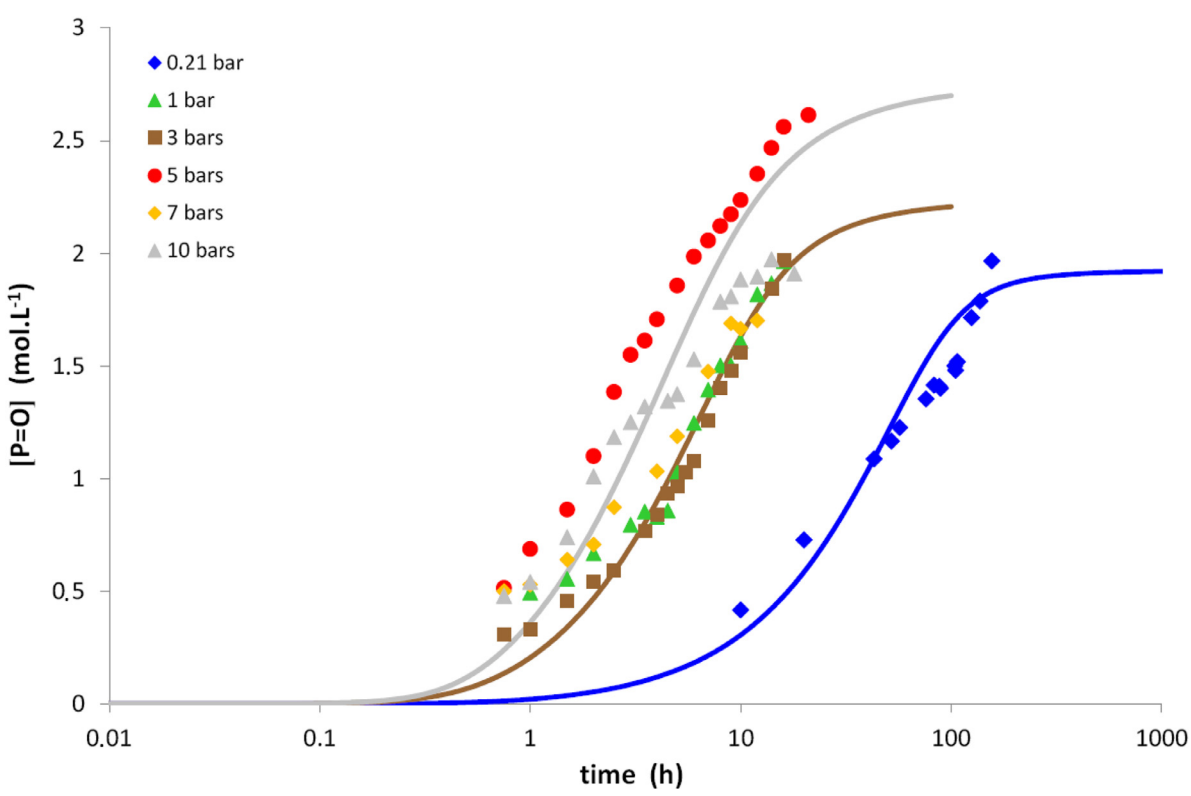

Fig. 7. Carbonyl build-up in 25 µm thick films of network no. 3 (DGEBF-CAF) at 150 °C between 0.21 (ambient air) and 10 bars of oxygen. Comparison between some simulations with Eq. (9) (solid lines) and experimental data (points).

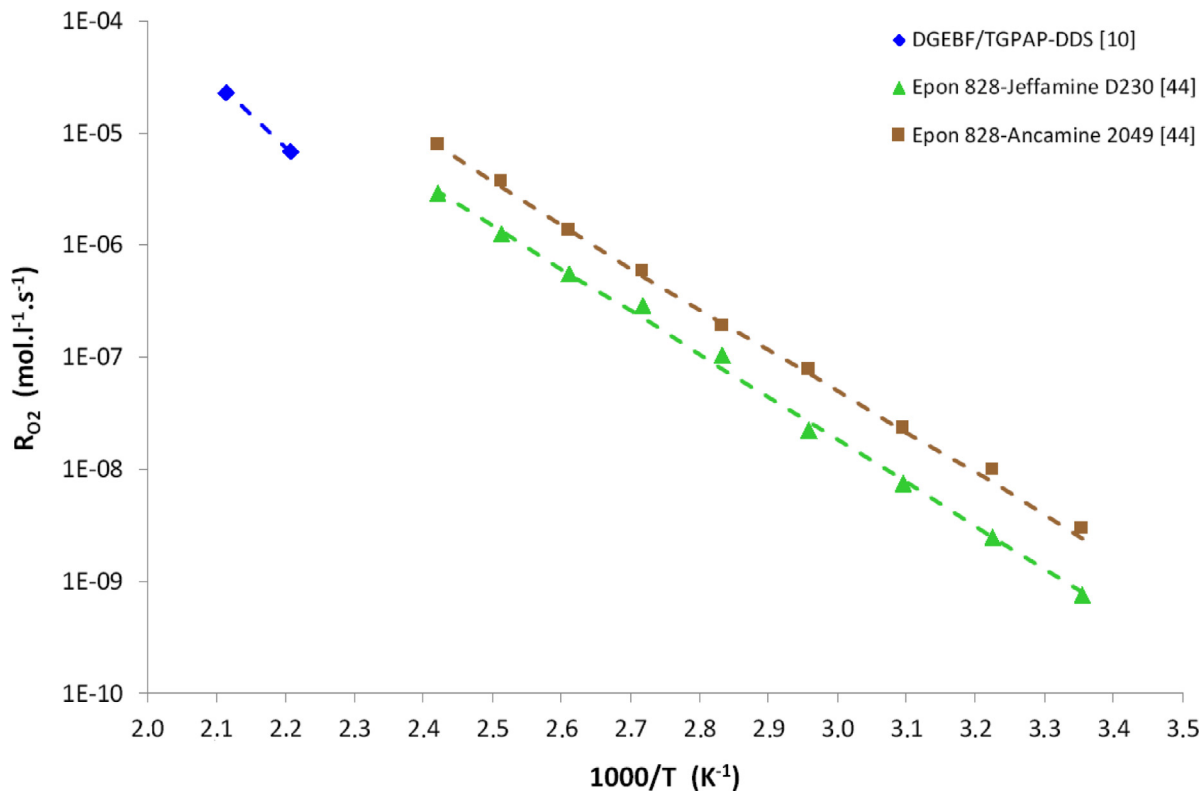

Fig. 8. Arrhenius graphs between 25 and 200 °C of the maximal oxidation rate under 0.166 bar of oxygen for 100 µm thick films of networks no. 1 and 2 (Epon 828-Jeffamine D230 and Epon 828-Ancamine 2049, respectively), and 50 µm thick films of network no. 5 (DGEBF/TGPAP-DDS). Comparison between the simulations with Eq. (8) (solid lines) and literature data (points) [10,44].

130 °C $\leq$ T $\leq$ T_g + 45 °C). Maximal oxidation rates were calculated with Eq. (8) between 25 and 140 °C under 0,166 bar of oxygen for networks no. 1 and 2, and at 180 and 200 °C under 0,166 bar of oxygen for network no. 5. Here again, it can be seen that the kinetic model satisfyingly predicts the effect of temperature on the oxidation kinetics of these three EPO-DA networks throughout this wide temperature range.

For a sake of brevity and clarity, only the rate constants and formation yields used for the simulations at the two highest temperatures, for each EPO-DA under study, are reported in Table 6. The parameter values obtained at all other temperatures are available in Appendix A for networks no. 1 and 2.

These new results call for the following additional comments. As expected, the gap between the oxidation kinetics of the EPO-DA networks and aliphatic polyamides continues to narrow when increasing the temperature of exposure, and ends up disappearing almost totally when equalizing and exceeding the glass transition temperature of EPO-DA networks. As an example, at T = T_g + 30 °C for network no. 1, k_6 and k_3 take almost the same values than in aliphatic polyamides (at T $\approx$ T_g + 100 °C).

5. Discussion

The values of the rate constant k_6 determined for the six EPO-DA networks under study have been plotted as a function of the reciprocal temperature 1/T in Fig. 9. The values found for aliphatic polyamides in a previous study [37] have been added for comparison. The vertical solid straight-lines indicate the position of the T_g of the different materials.

At first glance, it would seem that the effect of molecular mobility causes only a shift of the different curves along the abscissa axis. Thus, if assuming that k_6 obeys an Arrhenius law, the molecular mobility would only affect the pre-exponential factor of k_6 (i.e. the frequency of chemical events between peroxy radicals) and not its activation energy.

To check this assumption, the values of k_6 were plotted as a function of the difference (1/T – 1/T_g), which amounts to positioning 1/T_g of all materials on the ordinate axis passing through the origin (i.e. at 1/T = 0). As expected, the resulting shift along the abscise axis of the different curves allows obtaining a single master curve for k_6 (see Fig. 10), whose the general shape can be satisfyingly described by the statistical model of Mahieux and Reifsnider [60,61]. Although this model was firstly developed for simulating the temperature dependence of the storage modulus in large temperature range, due to the presence of several thermodynamic transitions such as: secondary relaxations, glass transition, melting, etc., it seems to be perfectly suited for this study. Around the glass transition temperature, this model can be rewritten as follows:

$$k_6 = k_{6r} + (k_{6v} + k_{6r}) \times \ \mathrm{Exp}\left[-\left(\frac{1/T - 1/T_v}{1/T_r - 1/T}\right)^m\right] \tag{18}$$

where T_v and T_r are the temperatures delimiting the action zone of the glass transition from the fully glassy and rubbery domains, respectively; m is a statistical parameter related to the width of the action zone; and k_{6v} and k_{6r} are the values of k_6 in the fully glassy and rubbery domains, respectively.

Its numerical application to the master curve of Fig. 10 allows the determination of the statistical parameter (m $\approx$ 1.3) and the temperature dependence of k_6 on both sides of the glass transition temperature. It was found that k_6 tends to be almost independent of temperature in the rubbery domain:

$$k_{6r} = 1.4\ 10^{10}\ \mathrm{L.mol^{-1}.s^{-1}} \tag{19}$$

In contrast, k_6 obeys an Arrhenius law in the glassy domain:

$$k_{6v} = 1.4\ 10^{5}\ \mathrm{Exp}\left[-\frac{16\ 000}{R}\left(\frac{1}{T} - \frac{1}{T_g}\right)\right]\mathrm{L.mol^{-1}.s^{-1}} \tag{20}$$

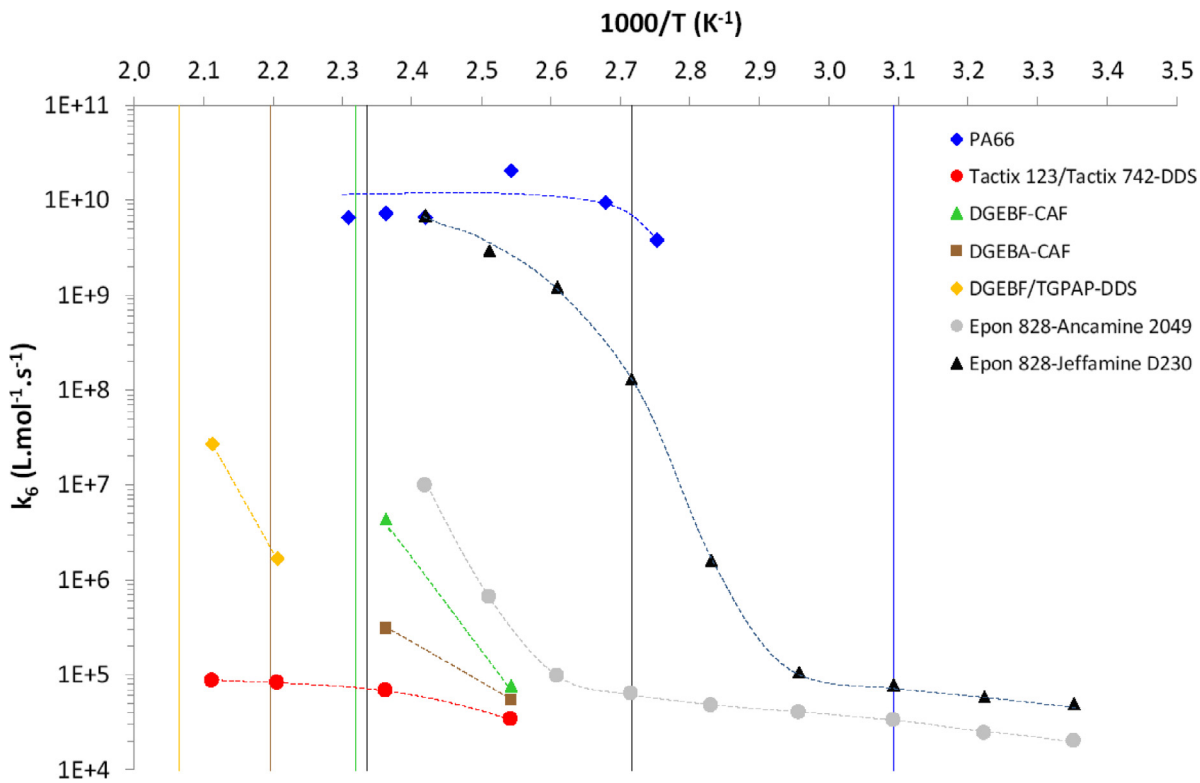

Fig. 9. Arrhenius graphs between 25 and 250 °C of the rate constant k_6 for the six EPO-DA networks under study and aliphatic polyamides. The vertical solid straight-lines indicate the position of the T_g of the different materials.

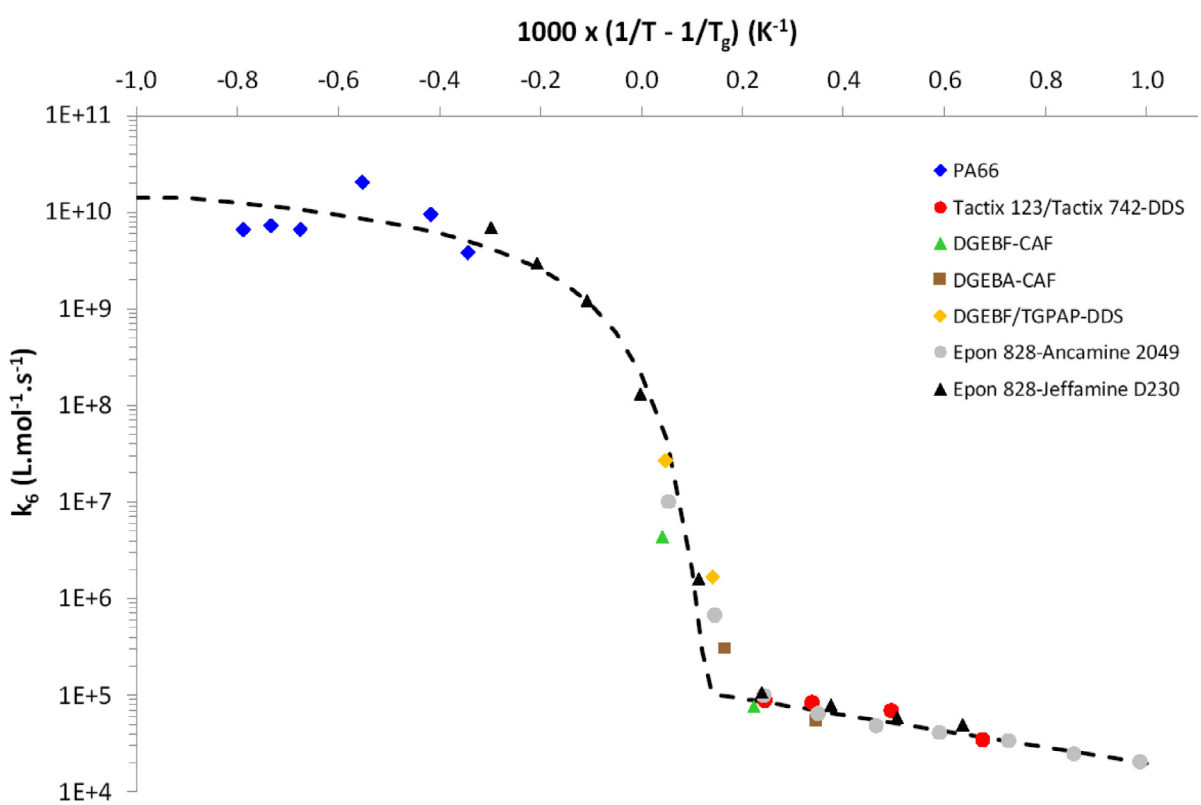

Fig. 10. Master curve around the glass transition temperature for the rate constant k_6 of EPO-DA networks and aliphatic polyamides. Modeling of the impact of the thermodynamic transition with Eq. (18).

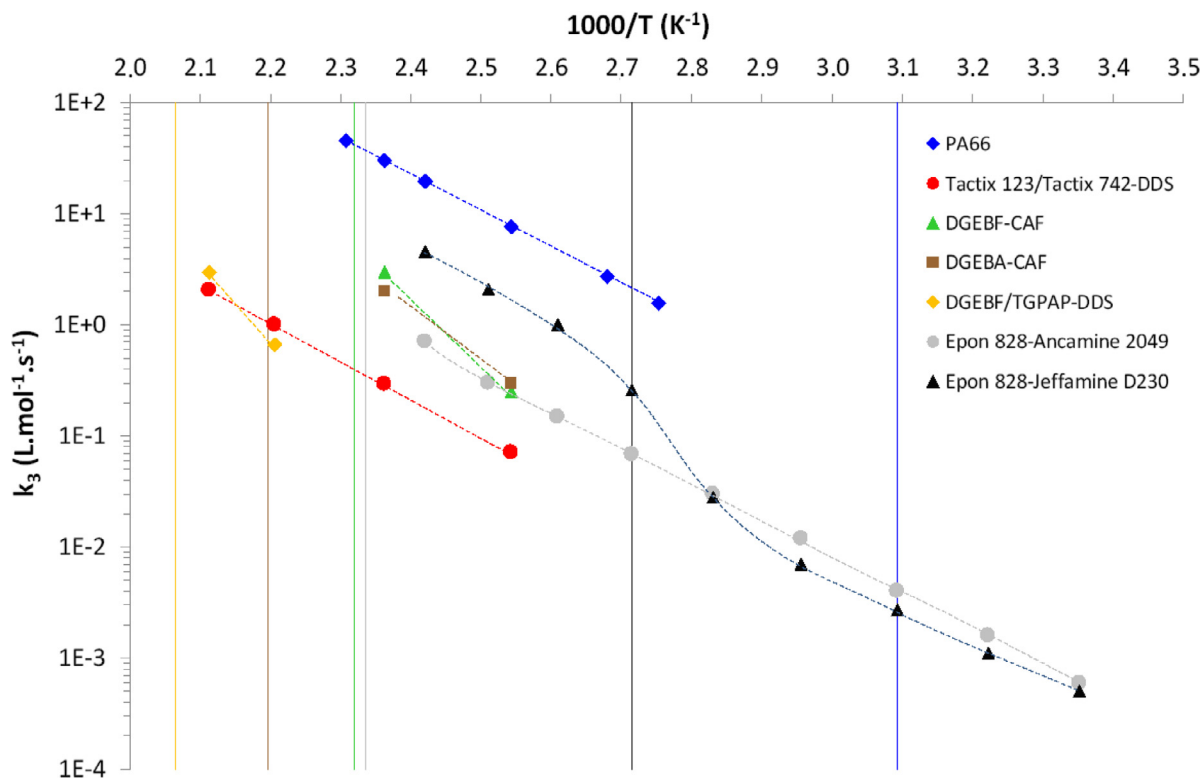

Fig. 11. Arrhenius graphs between 25 and 250 °C of the rate constant k_3 for the six EPO-DA networks under study and aliphatic polyamides. The vertical solid straight-lines indicate the position of the T_g of the different materials.

It has been tried to apply the same methodology to rate constant k_3. However, in this case, the molecular mobility does not cause a simple shift of the different curves along the abscissa axis. Indeed, in Fig. 11, it can be noted that some curves are already very close to each other, while the corresponding EPO-DA networks have very different values of T_g. This the case for networks no. 2, 3 and 4 on one hand, and networks no. 5 and 6 on the other hand.

According to Korcek et al.[18], the pre-exponential factor k_{30} of the rate constant k_3 depends above all on the dissociation energy of the C-H, but also secondarily on the reactivity of the involved peroxy radical $PO_2^{\bullet}$. However, in the previous section, it has been shown that their reactivity (through k_6) is significantly impacted by the molecular mobility. As a consequence, k_3 is expected to show a little more complicated variation with T_g than k_6 in both the rubbery and glassy domains (see Eqs. 19 and 21).

At first, the values of k_3 were plotted as a function of the difference $(1/T - 1/T_g)$, as previously done for k_6. As expected, the resulting shift along the abscise axis of the different curves does not allow obtaining a single master curve for k_3 (see Fig. 12). However, if looking at the variation of k_{30} with the T_g of the different materials (most of the data are in glassy state), one founds that k_{30} increases exponentially with T_g

$$k_{30} \propto \ \mathrm{Exp}\left(\frac{T_g}{30}\right) \tag{21}$$

Then, the curve of aliphatic polyamides was chosen as the reference curve. Eq. 21 was used to shift along the ordinate axis all the curves of EPO-DA networks, thus obtaining a single master curve for k_3 (see Fig. 13). As for k_6, the general shape of k_3 can be satisfyingly described by the statistical model of Mahieux and Reifsnider [60,61]:

$$k_3 = k_{3r} + (k_{3v} + k_{3r}) \times \ \mathrm{Exp}\left[-\left(\frac{1/T - 1/T_v}{1/T_r - 1/T}\right)^m\right] \tag{22}$$

where k_{3v} and k_{3r} are the values of k_3 in the fully glassy and rubbery domains, respectively.

Its numerical application to the master curve of Fig. 13 allows the determination of the statistical parameter ($m \approx 0.9$) and the temperature dependence of k_3 on both sides of the glass transition temperature. It was found that k_3 obeys an Arrhenius law with the same activation energy on both sides of the glass transition temperature. In the rubbery domain:

$$k_{3r} = 1.0\ 10^{-1}\ \mathrm{Exp}\left(\frac{T_g - 50}{30}\right) \mathrm{Exp}\left[-\frac{64\ 000}{R}\left(\frac{1}{T} - \frac{1}{T_g}\right)\right] \mathrm{L.mol^{-1}.s^{-1}} \tag{23}$$

In the glassy domain:

$$k_{3v} = 1.9\ 10^{-2}\ \mathrm{Exp}\left(\frac{T_g - 50}{30}\right) \mathrm{Exp}\left[-\frac{64\ 000}{R}\left(\frac{1}{T} - \frac{1}{T_g}\right)\right] \mathrm{L.mol^{-1}.s^{-1}} \tag{24}$$

The scattering of data in the glassy domain appears to be sufficiently narrow (over only one decade) to allow the use of a single kinetic model for the whole family of EPO-DA networks. If neglecting any experimental error, this scattering can be due to three sources:

i) Errors in the calculation of the concentration of oxidation sites.
ii) Differences in the reactivity of oxidation sites (i.e. between oxy-methylene, amino-methylene and methanol groups) and

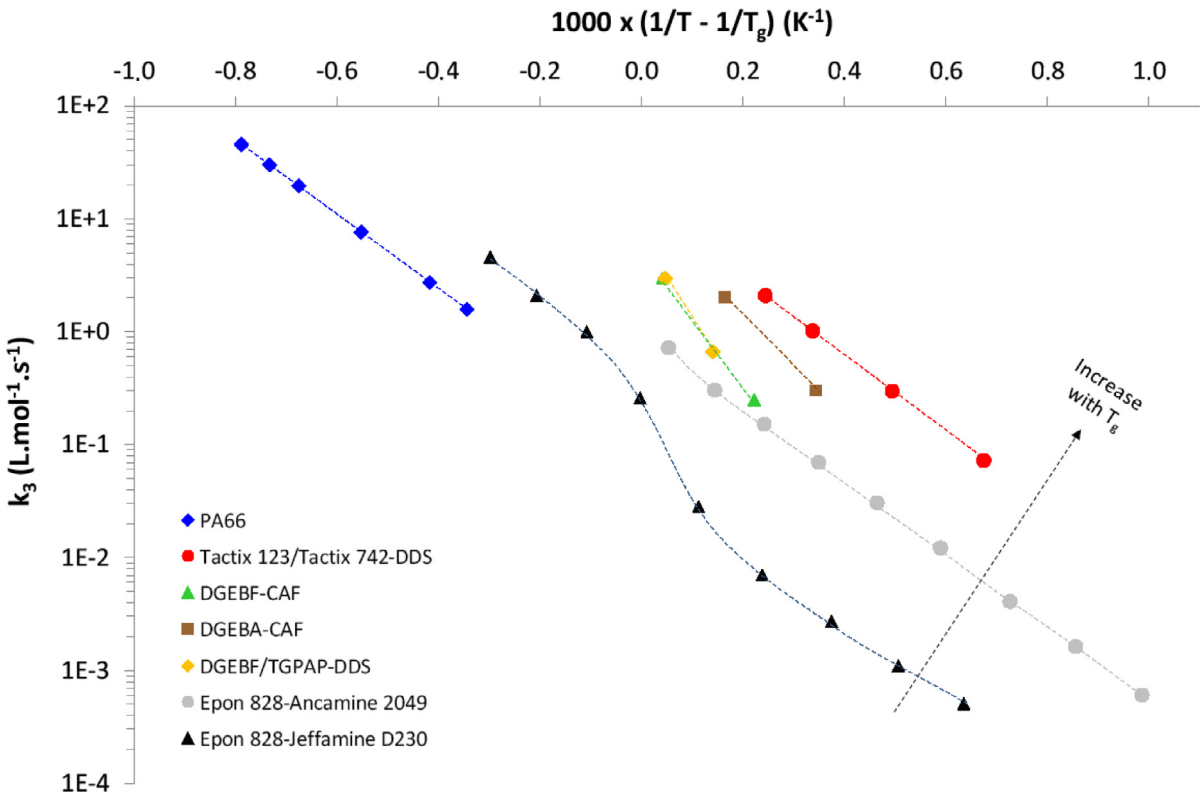

Fig. 12. Result of the shift along the abscise axis of the curves of Fig. 11. It can be noted an increase k_{30} with the T_g of the different materials.

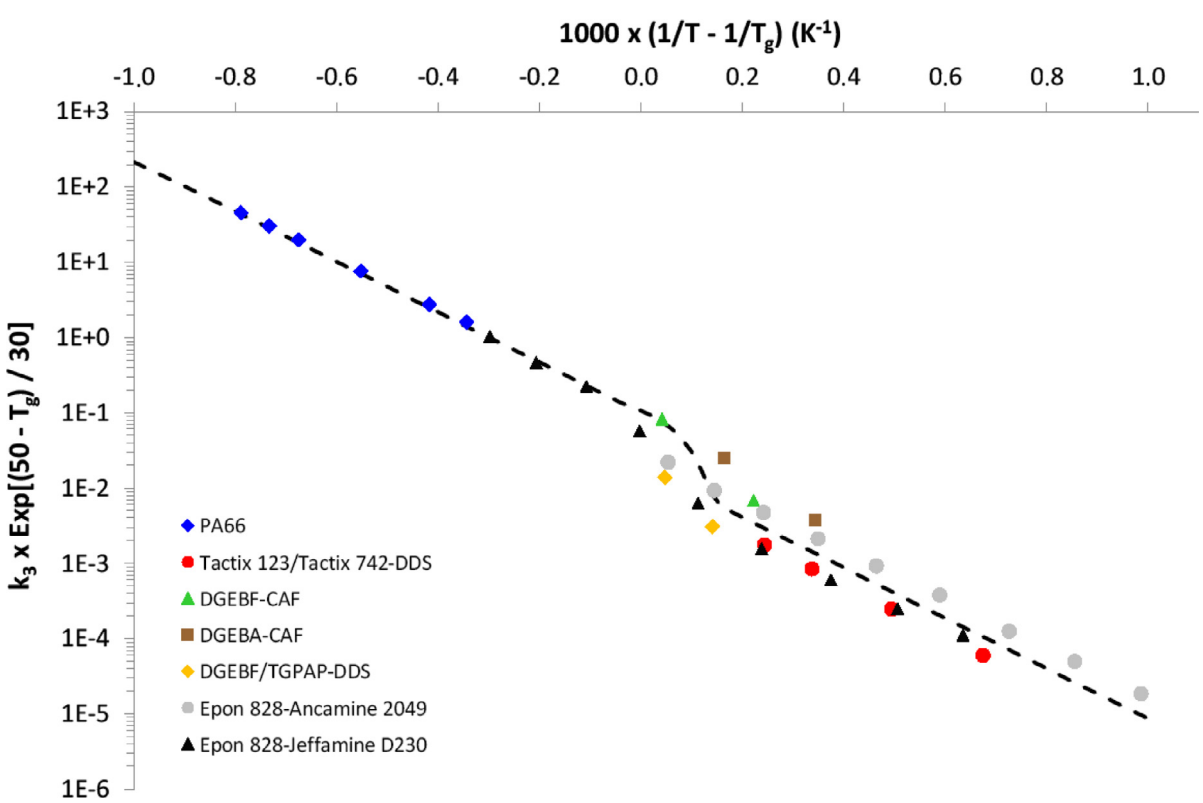

Fig. 13. Master curve around the glass transition temperature for the rate constant k_3 of EPO-DA networks and aliphatic polyamides. Modeling of the impact of the thermodynamic transition with Eq. (22).

therefore also, differences in the reactivity of the resulting peroxy radicals.

iii) A possible loss of aromaticity leading to the formation of highly oxidizable aliphatic structures during thermal aging.

The impact of two first assumptions on the values of k_3 should be very limited (of a factor lower than 2) and thus, not allow a full explanation of the width of data cloud. In contrast, the last assumption should be carefully considered, in particular epoxies cross-linked with an aromatic hardener, because it could theoretically impact by several orders of magnitude the values of k_3. Such a radical recombination has already been evidenced in a highly aromatic polymer, for instance in poly(ether ether ketone) [62].

6. Conclusion

The kinetic model developed for the thermal oxidation of polymethylenic substrates in previous studies [22,31-37]was successfully generalized to EPO-DA networks in the present study. Its numerous parameters were determined by applying a "step by step" procedure combining experiment and simulation.

It was found that the oxygen transport properties depend (i.e. oxygen diffusion and solubility) on the aromaticity of the EPO-DA network, whereas the rate constants of the apparent termination of peroxy radicals (k_6) and the propagation of oxidation (k_3) are highly impacted by the molecular mobility around the glass transition temperature (T_g). The introduction of the effect of molecular mobility into the Arrhenius laws of k_6 and k_3 allowed building master curves and finally, proposing a single kinetic model for the whole family of EPO-DA networks. In addition, the sharp variation of both rate constants with temperature within the glass transition zone (i.e. when passing from glassy to rubbery state) was successfully described using the statistical model of Mahieux and Reifsnider [60,61], although initially developed for the storage modulus. It is thus clear that the molecular mobility plays a key role in both the mechanical behavior and in the durability around the glass transition temperature of EPO-DA networks.

Despite this apparent success, at least two main challenges remain to be met. The effect of aromaticity on oxygen transport properties is not well understood and would deserve an in-depth and specific study on a series of model EPO-DA networks, but also on a series of linear polymers having almost the same chemical composition than EPO-DA networks (e.g. polycarbonate, polysulfone, etc.).

Similarly, the effect of aromaticity on the thermal oxidation kinetics should be carefully considered because it could explain small behavioral differences observed between the different EPO-DA networks in the glassy state. In particular, a possible loss of aromaticity could certainly allow reducing the scattering of data observed on the master curve of k_3 (Fig. 13).

In its current form, the kinetic model can be now used to elucidate the oxidation behavior of many industrial materials exhibiting T_g gradients such as: thick structures in composite material and joints of glue in assemblies of metal parts with composite material structures.

Declaration of Competing Interest

The authors declare that they have no known competing financial interests or personal relationships that could have appeared to influence the work reported in this paper.

Appendix A

Tables A1–A2.

Table A.1
Values of the rate constants and formation yields used for modeling the thermal oxidation kinetics of networks no. 1 between 25 and 140 °C.

Network	Epon 828-Jeffamine D230 [T_g = 95 °C]								
T (°C)	25	37	50	65	80	95	110	125	140
k_{1u} (s^{-1})	2.6×10^{-10}	2.0×10^{-9}	1.5×10^{-8}	1.3×10^{-7}	8.9×10^{-7}	5.4×10^{-6}	2.8×10^{-5}	1.3×10^{-4}	5.4×10^{-4}
k_{1b} ($L.mol^{-1}.s^{-1}$)	3.3×10^{-7}	1.3×10^{-6}	5.5×10^{-6}	2.4×10^{-5}	9.4×10^{-5}	3.3×10^{-4}	1.0×10^{-3}	3.0×10^{-3}	8.0×10^{-3}
k_2 ($L.mol^{-1}.s^{-1}$)	10^8	10^8	10^8	10^8	10^8	10^8	10^8	10^8	10^8
k_3 ($L.mol^{-1}.s^{-1}$)	5.0×10^{-4}	1.1×10^{-3}	2.7×10^{-3}	7.0×10^{-3}	2.8×10^{-2}	2.6×10^{-1}	1.0	2.1	4.6
k_4 ($L.mol^{-1}.s^{-1}$)	8.0×10^{11}	8.0×10^{11}	8.0×10^{11}	8.0×10^{11}	8.0×10^{11}	8.0×10^{11}	8.0×10^{11}	8.0×10^{11}	8.0×10^{11}
k_5 ($L.mol^{-1}.s^{-1}$)	3.0×10^{11}	3.0×10^{11}	3.0×10^{11}	3.0×10^{11}	3.0×10^{11}	3.0×10^{11}	3.0×10^{11}	3.0×10^{11}	3.0×10^{11}
k_6 ($L.mol^{-1}.s^{-1}$)	4.9×10^4	5.9×10^4	7.8×10^4	1.1×10^5	1.6×10^6	1.8×10^8	1.2×10^9	2.9×10^9	6.9×10^9
γ_1 (%)	60	60	60	60	60	60	60	60	60
γ_4 (%)	50	50	50	50	50	50	50	50	50
γ_5 (%)	50	50	50	50	50	50	50	50	50

Table A.2
Values of the rate constants and formation yields used for modeling the thermal oxidation kinetics of networks no. 2 between 25 and 140 °C.

Network	Epon 828-Ancamine 2049 [T_g = 150–155 °C]								
T (°C)	25	37	50	65	80	95	110	125	140
k_{1u} (s^{-1})	2.6×10^{-10}	2.0×10^{-9}	1.5×10^{-8}	1.3×10^{-7}	8.9×10^{-7}	5.4×10^{-6}	2.8×10^{-5}	1.3×10^{-4}	5.4×10^{-4}
k_{1b} ($L.mol^{-1}.s^{-1}$)	3.3×10^{-7}	1.3×10^{-6}	5.5×10^{-6}	2.4×10^{-5}	9.4×10^{-5}	3.3×10^{-4}	1.0×10^{-3}	3.0×10^{-3}	8.0×10^{-3}
k_2 ($L.mol^{-1}.s^{-1}$)	10^8	10^8	10^8	10^8	10^8	10^8	10^8	10^8	10^8
k_3 ($L.mol^{-1}.s^{-1}$)	6.0×10^{-4}	1.6×10^{-3}	4.0×10^{-3}	1.2×10^{-2}	3.0×10^{-2}	6.8×10^{-2}	1.5×10^{-1}	3.0×10^{-1}	7.0×10^{-1}
k_4 ($L.mol^{-1}.s^{-1}$)	8.0×10^{11}	8.0×10^{11}	8.0×10^{11}	8.0×10^{11}	8.0×10^{11}	8.0×10^{11}	8.0×10^{11}	8.0×10^{11}	8.0×10^{11}
k_5 ($L.mol^{-1}.s^{-1}$)	3.0×10^{11}	3.0×10^{11}	3.0×10^{11}	3.0×10^{11}	3.0×10^{11}	3.0×10^{11}	3.0×10^{11}	3.0×10^{11}	3.0×10^{11}
k_6 ($L.mol^{-1}.s^{-1}$)	2.0×10^4	2.4×10^4	3.3×10^4	4.0×10^4	4.8×10^4	6.2×10^4	9.8×10^4	6.5×10^5	9.9×10^6
γ_1 (%)	60	60	60	60	60	60	60	60	60
γ_4 (%)	50	50	50	50	50	50	50	50	50
γ_5 (%)	50	50	50	50	50	50	50	50	50

References

[1] T. Dyakonov, P.J. Mann, Y. Chen, W.T.K. Stevenson, Thermal analysis of some aromatic amine cured model epoxy resin systems—II: Residues of degradation, Polym. Degrad. Stab. 54 (1) (1996) 67–83.

[2] P. Musto, G. Ragosta, P. Russo, L. Mascia, Thermal oxidative degradation of epoxy and epoxy-bismaleimide networks: Kinetics and mechanism, Macromol. Chem. Phys. 202 (18) (2001) 3445–3458.

[3] P. Musto, Two-dimensional FTIR spectroscopy studies on the thermal oxidative degradation of epoxy and epoxy−bis(maleimide) networks, Macromol 36 (9) (2003) 3210–3221.

[4] B. Mailhot, S. Morlat-Therias, M. Ouhioune, J.-L. Gardette, Study of the degradation of an epoxy/amine resin, Macromol. Chem. Phys. 206 (5) (2005) 575–584.

[5] F. Delor-Jestin, D. Drouin, P.Y. Cheval, J. Lacoste, Thermal and photochemical ageing of epoxy resin – Influence of curing agents, Polym. Degrad. Stab. 91 (6) (2006) 1247–1255.

[6] B. Dao, J. Hodgkin, J. Krstina, J. Mardel, W. Tian, Accelerated aging versus realistic aging in aerospace composite materials. I- The chemistry of thermal aging in a low-temperature-cure epoxy composite, J. Appl. Polym. Sci. 102 (5) (2006) 4291–4303.

[7] N. Longerias, M. Sebban, P. Palmas, A. Rivaton, J.-L. Gardette, Degradation of epoxy resins under high energy electron beam irradiation: Radio-oxidation, Polym. Degrad. Stab. 92 (12) (2007) 2190–2197.

[8] C. Galant, B. Fayolle, M. Kuntz, J. Verdu, Thermal and radio-oxidation of epoxy coatings, Prog. Org. Coat. 69 (4) (2010) 322–329.

[9] Y.-M. Pei, K. Wang, M.-S. Zhan, W. Xu, X.-J. Dhing, Thermal-oxidative aging of DGEBA/EPN/LMPA epoxy system: Chemical structure and thermal-mechanical properties, Polym. Degrad. Stab. 96 (7) (2011) 1179–1186.

[10] X. Colin, C. Marais, J. Verdu, A new method for predicting the thermal oxidation of thermosets. Application to an amine crosslinked epoxy, Polym. Test. 20 (7) (2001) 795–803.

[11] X. Colin, C. Marais, J. Verdu, Kinetic modelling and simulation of gravimetric curves. Application to the oxidation of bismaleimide and epoxy resins, Polym. Degrad. Stab. 78 (3) (2002) 545–553.

[12] J. Decelle, N. Huet, V. Bellenger, Oxidation induced shrinkage for thermally aged epoxy networks, Polym. Degrad. Stab. 81 (2) (2003) 239–248.

[13] X. Colin, C. Marais, J. Verdu, Kinetic modelling of the stabilizing effect of carbon fibre on thermal ageing thermoset matrix composites, Compos. Sci. Technol. 65 (2005) 117–127.

[14] M.-C. Lafarie-Frenot, J.-C. Grandidier, M. Gigliotti, L. Olivier, X. Colin, J. Verdu, J. Cinquin, Thermo-oxidation behaviour of composite materials at high temperatures: A review of research activities carried out within the COMEDI program, Polym. Degrad. Stab. 95 (6) (2010) 965–974.

[15] X. Colin, B. Fayolle, J. Cinquin, Nouvelles avancées en modélisation cinétique de la thermo-oxydation des matrices époxy-diamines, Mater. Tech.104 (2) (2016) paper no. 202.

[16] J. Cinquin, X. Colin, B. Fayolle, M. Mille, S. Terekhina, L. Chocinski-Arnault, M. Gigliotti, J.-C. Grandidier, M.-C. Lafarie-Frenot, M. Minervino, C. Cluzel, F. Daghia, P. Ladeveze, F. Zhang, Thermo-oxidation behavior of organic matrix composite materials at high temperatures, Adv. Aircr. Spacecr. Sci. 3 (2) (2016) 171–195.

[17] E. Ernault, J. Dirrenberger, E. Richaud, B. Fayolle, Prediction of stress induced by heterogeneous oxidation: Case of epoxy/amine networks, Polym. Degrad. Stab. 162 (2019) 112–121.

[18] S. Korcek, J.H.B. Chenier, J.A. Howard, K.U. Ingold, Absolute rate constants for hydrocarbon autoxidation. XXI. Activation energies for propagation and the correlation of propagation arte constants with carbon-hydrogen bond strengths, Can. J. Chem. 50 (14) (1972) 2285–2297.

[19] J.-P. Pascault, H. Sautereau, J. Verdu, R.J.J. Williams, Thermosetting Polymers, Marcel Dekker, New York, 2002.

[20] V. Langlois, L. Audouin, J. Verdu, P. Courtois, Thermooxidative aging of crosslinked linear polyethylene: Stabilizer consumption and lifetime prediction, Polym. Degrad. Stab. 40 (3) (1993) 399–409.

[21] L. Audouin, X. Colin, B. Fayolle, J. Verdu, Sur l'utilisation de la loi d'Arrhenius dans le domaine du vieillissement des polymères, Mater. Techn. 95 (2007) 167–177.

[22] N. Khelidj, X. Colin, L. Audouin, J. Verdu, C. Monchy-Leroy, V. Prunier, Oxidation of polyethylene under irradiation at low temperature and low dose rate. Part II- Low temperature thermal oxidation, Polym. Degrad. Stab. 91 (7) (2006) 1598–1605.

[23] T.R. Waite, Bimolecular reaction rates in solids and liquids, J. Chem. Phys. 32 (1) (1960) 21–23.

[24] N.M. Emanuel, A.L. Buchachenko, Chemical Physics of Polymer Degradtion and Stabilization, VNU Science Press, Ultrech, The Netherlands, 1987.

[25] E.T. Denisov, Polymer oxidation and antioxidant action, in: S. Halim Hamid (Ed.), Handbook of Polymer Degradation, Marcel Dekker, New-York, 2000, pp. 383–419. Chap. 9.

[26] X. Colin, C. Marais, J. Verdu, Thermal oxidation kinetics for a poly-(bismaleimide), J. Appl. Polym. Sci. 82 (14) (2001) 3418–3430.

[27] K. Abdeljaoued, Study of matrix thermal oxidation in carbon fibers-PMR-15 composites, PhD thesis, ENSAM, Paris, 1999.

[28] T. Devanne, A. Bry, L. Audouin, J. Verdu, Radiochemical ageing of an amine cured epoxy network. Part I: change of physical properties, Polymer (Guildf) 46 (1) (2005) 229–236.

[29] S. Terekhina, M. Mille, B. Fayolle, X. Colin, Oxidation induced changes in viscoelastic properties of a thermostable epoxy matrix, Polym. Sci. Ser. A 55 (10) (2013) 614–624.

[30] X. Colin, G. Teyssèdre, M. Fois, in: A. Boudenne, L. Ibos, Y. Candau, S. Thomas (Eds.), Ageing and Degradation of Multiphase Polymer systems, Dans Handbook of Multiphase Polymer Systems, Vol. 2/2, John Wiley & Sons Ltd, Chichester, 2011, pp. 797–841. Chap. 21.

[31] X. Colin, L. Audouin, J. Verdu, M. Rozental-Evesque, B. Rabaud, F. Martin, F. Bourgine, Aging of polyethylene pipes transporting drinking water disinfected by chlorine dioxide. I-Chemical aspects, Polym. Eng. Sci. 49 (7) (2009) 1429–1437.

[32] A. Mikdam, X. Colin, G. Minard, N. Billon, R. Maurin, A kinetic model for predicting the oxidative degradation of additive free polyethylene in bleach desinfected water, Polym. Degrad. Stab. 146 (2017) 78–94.

[33] X. Colin, M. Ben Hassine, M. Nait-Abdelaziz, Chemo-mechanical model for predicting the lifetime of EPDM rubbers, Rubber Chem. Technol. 92 (4) (2019) 722–748.

[34] M. Coquillat, J. Verdu, X. Colin, L. Audouin, R. Nevière, Thermal oxidation of polybutadiene. Part II-Mechanistic and kinetic schemes for additive free uncrosslinked polybutadiene, Polym. Degrad. Stab. 92 (7) (2007) 1334–1342.

[35] L.K. Nait-Ali, X. Colin, A. Bergeret, Kinetic analysis and modeling of PET macromolecular changes during its mechanical recycling by extrusion, Polym. Degrad. Stab. 96 (2) (2011) 236–246.

[36] G. Minard, X. Colin, Thermal ageing of a hybrid composite rod for next generation overhead power lines, J. Compos. Sci. 3 (4) (2019) article no. 103.

[37] C. El Mazry, M. Ben Hassine, O. Correc, X. Colin, Thermal oxidation kinetics of free additive polyamide 6-6, Polym. Degrad. Stab. 98 (1) (2013) 22–36.

[38] L. Achimsky, L. Audouin, J. Verdu, J. Rychly, L. Matisova-Rychla, On a transition at 80 °C in polypropylene oxidation kinetics, Polym. Degrad. Stab. 58 (3) (1997) 283–289.

[39] C. Decker, F.R. Mayo, H. Richardson, Aging and degradation of polyolefins. III–Polyethylene and ethylene–propylene copolymers, J. Polym. Sci.: Polym. Chem. Ed. 11 (1973) 2879–2898.

[40] N. Khelidj, X. Colin, L. Audouin, J. Verdu, C. Monchy-Leroy, V. Prunier, Oxidation of polyethylene under irradiation at low temperature and low dose rate. Part I- The case of "pure" radiochemical initiation, Polym. Degrad. Stab. 91 (7) (2006) 1593–1597.

[41] E. Hairer, G. Wanner, Solving Ordinary Differential equations. II-Stiff and Differential-Algebraic Problems, Springer, Berlin, 1991.

[42] X. Colin, L. Audouin, J. Verdu, Determination of thermal oxidation rate constants by an inverse method. Application to polyethylene, Polym. Degrad. Stab. 86 (2004) 309–321.

[43] E.A. Di Marzio, On the second-order transition of a rubber, J. Res. Natl. Br. Stand.: Sect. A 68 (1964) 611–617.

[44] M. Celina, A.R. Dayile, A. Quintana, A perspective on the inherent oxidation sensitivity of epoxy materials, Polymer (Guildf) 54 (2013) 3290–3296.

[45] E. Girard-Reydet, C.C. Riccardi, H. Sautereau, J.P. Pascault, Epoxy-aromatic amine kinetics. 1- Modeling and influence of diamine structure, Macromolecules 28 (1995) 7599–7607.

[46] V. Bellenger, C. Bouchard, P. Claveirolle, J. Verdu, Photo-oxidation of epoxy resins cured by non-aromatic amines, Polym. Photochem. 1 (1) (1981) 69–80.

[47] V. Bellenger, J. Verdu, Oxidative skeleton breaking in epoxy–amine networks, J. Appl. Polym. Sci. 30 (1) (1985) 363–375.

[48] A. Rivaton, L. Moreau, J.-L. Gardette, Photo-oxidation of phenoxy resins at long and short wavelengths. I- Identification of the photoproducts, Polym. Degrad. Stab. 58 (3) (1997) 321–332.

[49] M.St.C. Flett, Intensities of some group characteristic infra-red bands, Spectrochim. Acta 18 (1962) 1537–1556.

[50] W.-D. Domke, H. Steinke, Oxidative structures in polyolefins: FT-IR method of quantitative determination, J. Polym. Sci.: Part A: Polym. Chem. 24 (10) (1986) 2701–2705.

[51] J. Lacoste, D.J. Carlsson, Gamma-, photo-, and thermally-initiated oxidation of linear low density polyethylene: A quantitative comparison of oxidation products, J. Polym. Sci.: Part A: Polym. Chem. 30 (1992) 493–500.

[52] A. Barth, Infrared spectroscopy of proteins, Biochim. Biophys. Acta (2007) (1767) 1073–1101.

[53] M. Da Cruz, L. Van Schoors, K. Benzari, X. Colin, Thermo-oxidative degradation of additive free polyethylene. Part I- Analysis of the chemical modifications at molecular and macromolecular scales, J. Appl. Polym. Sci. 133 (18) (2016) 43287.

[54] C. Damian, E. Espuche, M. Escoubes, Influence of three ageing types (thermal oxidation, radiochemical and hydrolytic ageing) on the structure and gas transport properties of epoxy-amine networks, Polym. Degrad. Stab. 72 (3) (2001) 447–458.

[55] C. Damian-Pélissier, Réseaux polyépoxydes utilisés pour l'enrobage des déchets radioactifs : analyse du vieillissement en conditions de stockage et effets sur les propriétés diffusionnelles des matériaux, PhD thesis, Université Claude Bernard, Lyon 1, France, 1999.

[56] Y. Zahara, Dégradation des réseaux époxy−amine en ambiance nucléaire, PhD thesis, Arts et Métiers ParisTech, Campus de Paris, France, 2012.

[57] M. Celina, A. Quintana, N. Giron, A. Dayile, An Overview of the Inherent Oxidation Sensitivity and DLO Behavior of Epoxy materials, 30th Meeting of PDDG, Arts et Métiers ParisTech, Paris, 1-4 Sept. 2013.

[58] M. Celina, A. Quintana, Oxygen diffusivity and permeation trough polymers at elevated temperature, Polymer (Guildf) 150 (2018) 326–342.

[59] J. Delozanne, Durabilité des époxys. Application au collage structural aéronautique, Thèse de doctorat, Arts et Métiers ParisTech, Campus de Paris, France, 2018.
[60] C.A. Mahieux, K.L. Reifsnider, Property modeling across transition temperatures in polymers : a robust stiffness-temperature model, Polymer (Guildf) 42 (2001) 3281–3291.
[61] C.A. Mahieux, K.L. Reifsnider, Property modeling across transition temperatures in polymers: Application to thermoplastic systems, J. Mater. Sci. 37 (2002) 911–920.
[62] S. Giancaterina, A. Rossi, A. Rivaton, J.-L. Gardette, Photochemical evolution of poly(ether ether ketone), Polym. Degrad. Stab. 68 (2000) 133–144.